Answers to referees of the manuscript

A microphysics guide to cirrus clouds Part 1: Cirrus types
by M. Krämer et al.

First of all, we would like to thank both referees for the helpful and constructive comments leading to an improved version of the manuscript.
In the following, the referees comments are in black, while the authors answers to the comments are given in blue.

Answers to Referee 1

General Comments:

This paper is an excellent blend of theory and observations, and demonstrates how a Lagrangian ice particle tracking model (MAID) with detailed microphysics and aerosol- cloud interactions can be used to reveal potential dynamical and microphysical mechanisms when compared against observations. This is a potentially large contribution to our understanding of cirrus clouds. The paper is well organized and written with figures of high quality.

Thanks a lot !

(a) My main concern is that the Cirrus Guide may be over-generalized. For example, in Muhlbauer et al. 2014 (Impact of large-scale dynamics on the microphysical properties of midlatitude cirrus, JGR), they describe 4 principal cirrus categories and their physical and microphysical characteristics (e.g. altitude, temperature, updraft speed, relative humidity with respect to ice or RHi, ice water content or IWC, ice particle number concentration or Ni, and ice particle size distribution or PSD parameters), based on SPARTICUS data. The cirrus clouds were grouped into categories based on their large-scale dynamic characteristics (inferred from ECMWF ERA-Interim reanalysis and ground based radar), with most cirrus falling into the following 4 categories: (1) upper- level ridges, (2) subtropical jets, (3) anvil cirrus and (4) frontal cirrus. This makes their results amenable to comparison with the Cirrus Guide proposed.

Answer:

We appreciate this comment. Though we are aware of the SPARTICUS field campaign and the study of Muhlbauer et al. (JGR, 2014), we simply did not have the idea of a comparison. However, following the referees suggestion, we feel now that a description of the differences and similarities in both data sets is necessary, so we have included a new section (5.5).

The main difference between the data sets which leads to a seeming discrepancy between the two studies are the different lower limits of IWC, which are about 1 mg/m^3 for SPARTICUS and 0.001 mg/m^3 for the Cirrus Guide data. This is shown in the Figure below (Cirrus Guide Figure 2, right panel), where we plotted the SPARTICUS lower and upper IWC boundaries as the horizontal black lines.

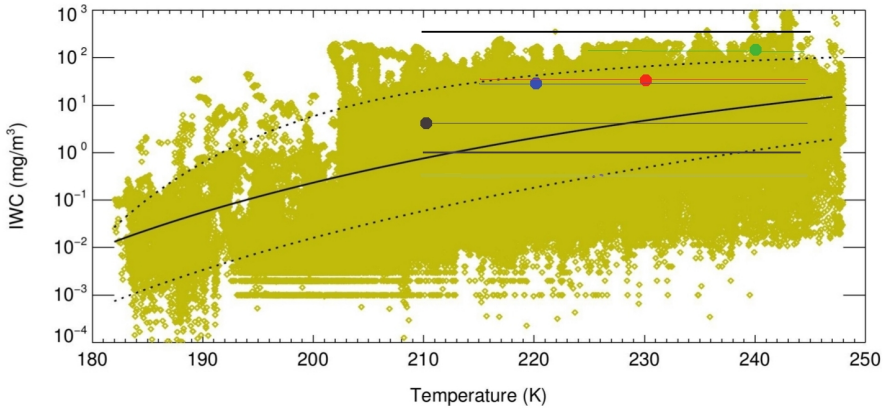

Cirrus Guide Figure 2 (right panel): IWC in mg/m^3 vs temperature. Black horizontal lines: SPARTICUS lower and upper IWC boundaries, drawn over the temparature range observed during SPARTICUS. Colored dots: peaks of IWC PDFs -for the temperature range indicated by the colored horizontal lines- of the 4 cirrus categories classified from SPARTICUS (black: ridge crest cirrus, blue: frontal cirrus, red: subtropical jet stream cirrus, green: anvil cirrus, Muhlbauer et al., Fig. 6).

(b) Ridge-crest cirrus (category 1) had relatively low IWC and relatively high Ni, and were fairly thin. This seems to contradict the proposed Cirrus Guide, which associates relatively high Ni with relatively high IWC for in situ cirrus. Table 2 of Muhlbauer et al. shows the days associated with each category, and the following NASA website:
http://www-angler.larc.nasa.gov/cgi-bin/site/showdoc?docid=4&cmd=flight- track-&exp=ARM-SPARTICUS-2009&ds=cp ,
gives satellite retrievals of SPARTICUS cloud physical properties, showing that the ridge-crest cirrus tend to be relatively thin with lower ice water path (IWP). One might expect such cirrus to belong to the slow updraft category of the Cirrus Guide, which would tend to predict low Ni and low IWC. Ridge-crest cirrus often have Ni $>$ 500 per liter, which is difficult to achieve through heterogeneous ice nucleation (Barahona & Nenes, 2009b, ACP). But in the Cirrus Guide, homogeneous ice nucleation producing high Ni is associated with fast updraft in situ cirrus.

Answer:
Due to the different IWC ranges of both data sets (see above figure), the classification of 'ridge-crest cirrus' as fairly thin with relatively low IWC and relatively high Ni is related to the SPARTICUS IWC range. With respect to the CIRRUS Guide IWC range, 'ridge-crest cirrus' are rather thick with relatively high IWC and relatively high Ni, thus matching the in-situ origin, fast updraft cirrus category which produces a high ice crystal number Ni by homogeneous freezing. We would conclude here a good agreement in the classification of both studies. For more detail see new Section 5.5.

(c) Muhlbauer et al. also found that PDFs of cloud updraft did not differ between the above 4 cirrus categories, indicating that cloud updraft was a poor predictor for explaining the microphysical variability in cirrus. The Cirrus Guide invokes cloud updraft as a key parameter for explaining different types of cirrus.

Answer:
The most frequent observations in the Muhlbauer et al. paper are in the higher IWC range above the median IWC line, which also means higher updrafts. This can be seen in Figure 7 of the Cirrus Guide (one panel is shown below; compare colored points in the above Figure):

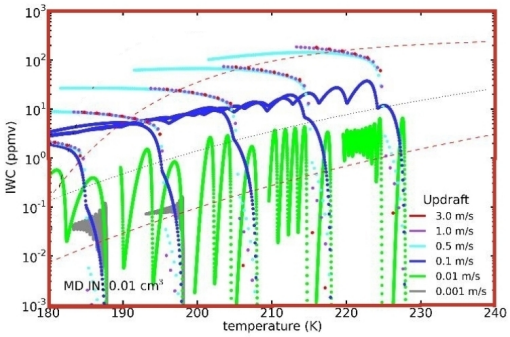

Cirrus Guide Figure 7: example of MAID IWCs

So we think the finding of Muhlbauer et al. is consistent for the high IWC range: here, it is not the updraft driving the different cirrus types that we call 'in-situ' and 'liquid-origin' cirrus. However, as can be seen in Figure 7, the driver of the in-situ cirrus with low and high IWC (in the Cirrus Guide parameter range) is updraft. For more detail see new Section 5.5.

(d) On the other hand, the anvil cirrus category and description in Muhlbauer et al. appears consistent with the description of anvil cirrus in the Cirrus Guide, which places anvil cirrus in the liquid origin cirrus category.

Answer: Yes

(e) Since there appear to be differences in the conclusions reached in the proposed Cirrus Guide and in Muhlbauer et al., this reviewer recommends an extensive discussion contrasting the two studies. There may be other differences not mentioned here.

Answer:
As mentioned in the answers to comment (a) and (b), we see that the studies compare well when taking into account the different IWC ranges. See also new Section 5.5.

(f) Another factor affecting cirrus cloud characteristics is their stage of evolution. The authors may want to consult papers by Minghui Diao et al. (e.g. Evolution of ice crystal regions on the microscale based on in situ observations, GRL, 2013;

Hemispheric comparison of cirrus cloud evolution using in situ measurements in HIAPER Pole-to- Pole Observations, GRL, 2014; Distributions of ice supersaturation and ice crystals from airborne observations in relation to upper tropospheric dynamical boundaries, JGR, 2015). The question comes whether the observations are reflecting a certain stage of cloud evolution or whether they are seeing a distinct type of cirrus. This topic could be relevant to the Cirrus Guide.

Answer:

It is not possible to directly assign the stage of cirrus evolution to aircraft observations (see also the introduction section of the paper). Thus, the observations present a mixture of evolution stages and cirrus types. It was the aim of the study to track cirrus IWC development with temperature by means of model simulations, compare with observations and then assign to a certain degree cirrus microphysics and formation mechanisms to the observations.

We think that we have shown that this is possible -to a certain degree-, since for in-situ cirrus in the slow updraft region the IWC and temperature changes only very slowly during the cirrus evolution and in the fast updraft region IWC reaches quickly a certain level and does not greatly change afterwards during the cirrus lifetime, i.e. the IWC does not greatly vary during the cirrus development and is not as sensitive to atmospheric variations as ice crystal numbers - a reason to choose IWC as major parameter for this study. The liquid-origin cirrus stage of development - they are aged, completely glaciated mixed clouds. In Figure 11 of the Cirrus Guide we have shown a data set where we excluded all data points with $RH_{ice} < 95\%$, since then ice crystals are in the evaporating stage and the IWCs become lower - consequently most of the very low IWC disappear from this diagram. These data points might be used to identify old evaporating cirrus, however, we feel that we do not want to add more figures to the paper.

With regard to the studies of Minghui Diao et al: we do not see how to relate these studies to ours since they discuss different parameters and use a completely different approach for their study.

Major Comments:

1. Section 2, page 31541: The paper would be enhanced if it included the SPARTICUS (2010) and recent ATTREX (near Guam) field campaign data. Both campaigns used modern probes (2D-S, FSSP, Hawkeye) and algorithms that minimize shattering where IWC can be calculated as a PSD integrated quantity (a practice used in this paper). SPARTICUS continuously sampled continental synoptic and anvil cirrus over a 6-month period, producing excellent statistics on cirrus cloud microphysical properties. It appears that most cirrus were sampled over land in this study (Fig. 1), making the ATTREX sampling over the western Pacific of greater interest. Enough field campaigns are already included in this study to lend sufficient credibility to the results, but it is possible something new would be revealed by including these two field campaigns.

Answer:
For the reason discussed above - the different IWC range of SPARTICUS and the Cirrus Guide - we think it is better to discuss/compare the two studies seperately and not to include the SPARTICUS data set here.

During the ATTREX campaign a large data set of TTL cirrus is sampled with advanced instrumentation, as the referee has stated. IWC is measured by using a combination of total and gas phase water covering the same range as in our study. However, these data will become public after the first publication which will appear soon.

We are working on a new climatology using only advanced cirrus measurements, based on the Cirrus guide data set together with the ATTREX data. In this study, we will show statistical analysis and geographical and altitude distribution of all cirrus parameters (IWC, N_{ice}, R_{ice} and RH_{ice} in around cirrus). So for this study we prefer not to include ATTREX.

2. Section 2.1, lines 13-20: It would be interesting to compare IWC calculated in this way to IWC calculated using the new approach described in Erfani and Mitchell (2015, ACPD), especially for D $<$ 200 microns.

Answer:
We have compared the Mass-Dimension relations of Mitchell et al. (JAS, 2010) and the new ones derived by Erfani and Mitchell (ACPD, 2015) in the below Figure; the relations are very similar, which gives us confidence in our calculation of IWCs from PSDs. This is also mentioned now in the paper (new page 6).

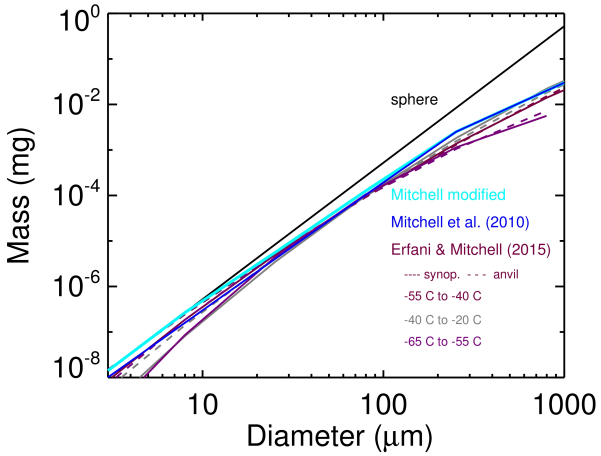

3. Section 4.1 and Fig. 5: Do the minimums (e.g. regarding Rice, etc.) indicate model initialization points? Please make it clear how this and other figures were produced using the MAID model.

Answer:
The minimum values appear when the first ice crystals form (hom. or het.) in the model, i.e. there is no model initialization point except of the water activity where the ice nucleates. This is also mentioned now in the paper (new page 11).

4. Section 4.2.2, first 6 lines: Here it becomes evident that cirrus lifetime actually refers to the lifetime of a cloud parcel. This distinction should be made early in the paper to avoid confusion.

Answer:
We added directly here (new page 16): '(note here that for such cases our simulations represent one cloud parcel passing the wave)', because we feel that this is the best place to explain the point raised by the referee. We also added at the beginning of the MAID description (new page 10): 'MAID simulates parcels of ice clouds where the ice crystals form directly from the gas phase ...'.

5. Section 4.2.3; TTL cirrus: Ni predicted here are < 1 per liter, whereas in Spichtinger and Krämer (2013, ACP) Ni for TTL cirrus averages ~ 30 per liter. This should be addressed.

Answer:
This is a good comment - however, it was not the idea to match the most frequent N_{ice} (~ 30 per liter) simulated in the study of Spichtinger and Krämer (2013) to and explain the observed frequency of occurence distribution of N_{ice}. Here, we show only one case of cirrus development, resulting from a specific vertical velocity and IN number. So an agreement between the two N_{ice} numbers can not be expected.
We added to the text (new page 17): 'Note, however, that the sensitivity case simulated here produces lower N_{ice} than the averge concentration of 0.03 cm^{-3} reported by Spichtinger and Krämer (2013).'

6. Page 31557, lines 24-26: This sentence could be somewhat confusing if a reader thinks that anvil cirrus are considered here (which are very common). Perhaps it should be stated here that anvil cirrus will be addressed later as belonging to another category.

Answer:
Thanks for that comment, we added on page 21: '... (note here that "fast updraft" does not include convection in the simulations; "convective" or "anvil" cirrus will be addressed later in Section 5.4 and 5.5).'

7. Page 31565, last sentence of paper: Anvil cirrus are liquid origin cirrus and are hypothesized here to have a net radiative cooling effect. I suggest that the authors look at Fig. 4 in Fu et al. (2002, ACP; Tropical cirrus and water vapor: an effective Earth infrared iris feedback?), showing net cloud radiative forcing as a function of cloud top height and optical depth. Fig. 4. of Fu et al. indicates that many tropical anvils, given their height, could have a warming effect if their optical depth is less than ~ 8 or 10 (which is quite common I think).

Answer:
The intention of the sentence was not to state that liquid origin (and thus anvil) cirrus have a cooling effect in general, but that only thick cirrus belonging to the fast updraft in-situ and liquid origin cirrus have the potential to cool - which is in agreement with the study of Fu et al. (ACP, 2002). To avoid this misunderstanding,

we reformulated the sentence to (see new page 30):

'..., we hypothesize here that on average the physically and optically thinner in-situ slow updraft cirrus cause a warming effect, while only thick fast updraft in-situ and particularly thick liquid origin cirrus have the potential to cool.'

Minor Comments:

1. Page 31539, line 26: Diameter and radius are not measured and they refer to a sphere; ice crystals are generally non-spherical. Consider another size descriptor, such as length or maximum dimension.

Answer:
This statement refers to measurements in cirrus in general and not specifically those of this study. To make that more clear, we changed the sentence to 'The most common parameters that are measured in cirrus clouds – besides the meteorological variables – are ice water content (IWC), ice crystal number (N_{ice}), crystal size and shape as well as relative humidity (with respect to ice, RH_{ice}).

On new page 13, footnote 5, we define now: 'The mean mass radius R_{ice} = IWC/N_{ice} is used for the representation of the model results for particle size, because it is comparable to the established cloud effective radius R_{eff}.'.

2. Page 31546, line 4: lesser → less? lesser overall → reduced overall?

Answer: Changed

3. Page 31555, line 7: warmer → all?

Answer:
We changed the sentence to: '... in particular at warmer temperatures, ...'

Additional Comment:

In regards to the review posted on 23 November, one sentence reads "On the other hand, the anvil cirrus category and description in Muhlbauer et al. appears consistent with the description of anvil cirrus in the Cirrus Guide, which places anvil cirrus in the liquid origin cirrus category." This statement is only partially correct. The Cirrus Guide description of anvil cirrus as liquid origin cirrus (having relatively high IWC and Ni) is consistent with the Muhlbauer et al. (2014) to the extent that anvil cirrus in Muhlbauer et al. have relatively high IWC, but Ni (ice particle number concentration) for anvil cirrus in Muhlbauer et al. is not relatively high, with peak Ni for other cirrus categories being higher than the peak Ni for anvil cirrus. Perhaps the IN concentrations in the vicinity of anvil cirrus are generally sufficient to prevent in-cloud RHi levels from reaching the threshold for homogeneous ice nucleation under most conditions (see Cziczo et al., 2013, Science), generally limiting Ni to < 500 per liter (Barahona & Nenes, 2009b, ACP).

Answer:
In the new manuscript, Section 5.5 (new pages 27pp), Muhlbauer and the Cirrus Guide are compared and with respect to the above comment we conclude: '... From the few observations we have, we can confirm that fast updraft in-situ cirrus (ridge crest in Muhlbauer et al., 2014) have a lower IWC but higher Nice than liquid origin cirrus (frontal, subtropical jet stream and anvil cirrus in Muhlbauer et al., 2014).

Answers to Referee 2

This work combines a comprehensive set of observations and trajectory model simulations to categorize cirrus clouds. The manuscript contributes to advancing our understanding of cirrus clouds, and it is suitable for ACP. I recommend publication of the manuscript, and suggest a few revisions that the authors may wish to consider to improve the manuscript.

Thanks a lot !

1) The trajectory parcel simulations cannot capture dynamical processes such as shear, entrainment, and cloud radiation-dynamics interactions. It would be helpful to mention these limitations of the parcel modeling approach compared with cloud-resolving model simulations. In fact, these dynamical processes tend to reduce the ice number concentrations below the initial values obtained by nucleation (Dinh et al., 2012, 2014). This could explain why Nice obtained by MAID can be higher than observations as seen in Fig. 5.

Answer

Thanks again for mentioning that point - we directly implemented your description of the limitations into the manuscript (new page 11). However, we think that the MAID N_{ice} quite nicely fit into the range of observations, though a reduction of N_{ice} by cloud radiation-dynamics interactions might have occured. Simulated N_{ice} distinctly higher than the observations are only seen at higher vertical velocities (1 m/s and larger) and lower temperatures ($\sim<$ 205 K), conditions which are not likely to occur in the atmosphere. Anyhow, we include these trajectories in the plot to give a complete picture.

2) The ice water content and ice number concentration have been categorized based on temperature. Is altitude an equivalent independent parameter for cirrus categorization? Specifically, do liquid-origin cirrus clouds occur at higher temperatures and equivalently lower altitudes, and in-situ cirrus clouds occur at lower temperatures and equivalently higher altitudes?

Answer

Yes, since altitude and temperature are related to each other, altitude could be also a parameter for categorazation. And indeed liquid origin cirrus are found at lower altitudes (higher temperatures) than in-situ origin cirrus. This is decribed in Luebke et al. (ACPD, 2015), which is a companion paper of this study (cited at the respective places of the manuscript

'The origin of midlatitude ice clouds
and the resulting influence on their microphysical properties'

(http//www.atmos-chem-phys-discuss.net/acp-2015-956/)

3) The manuscript focuses only on cirrus microphysics, but could potentially have a broader impact if the authors provide calculations of the cloud radiative properties. For example, it would be useful to have an additional panel/figure that

shows the cloud radiative heating rate (K/day) based on the ice number concentration, ice crystal radius, and cloud extinction in Fig. 12.

Answer

A good point - we have performed calculations of the radiative properties of the two cirrus types which were recently completed and confirm that only liquid origin cirrus have a potential for cooling. We discussed if we should include the results in this paper, but decided to keep this manuscript as short as possible and concentrated on the microphysics. We mention now the future work at the end of the paper in the conclusions.

References

T. Dinh, D. R. Durran, and T. Ackerman. Cirrus and water vapor transport in the tropical tropopause layer Part 1 A specific case modeling study. Atmos. Chem. Phys., 12(20) 97999815, 2012. doi:10.5194/acp-12-9799-2012.

T. Dinh, S. Fueglistaler, D. Durran, and T. Ackerman. Cirrus and water vapour transport in the tropical tropopause layer Part 2 Roles of ice nucleation and sedimentation, cloud dynamics, and moisture conditions. Atmos. Chem. Phys., 14(22) 1222512236, 2014. doi:10.5194/acp-14-12225-2014.

Manuscript prepared for Atmos. Chem. Phys. Discuss.
with version 2014/09/16 7.15 Copernicus papers of the LaTeX class copernicus.cls.
Date: 4 February 2016

A microphysics guide to cirrus clouds – Part 1: Cirrus types

M. Krämer[1], C. Rolf[1], A. Luebke[1,a], A. Afchine[1], N. Spelten[1], A. Costa[1], J. Meyer[9], M. Zöger[2], J. Smith[3], R. Herman[4], B. Buchholz[5], V. Ebert[5], D. Baumgardner[6], S. Borrmann[7], M. Klingebiel[7], and L. Avallone[8,a]

[1]Research Center Jülich, Institute for Energy and Climate Research (IEK-7), Jülich, Germany
[2]DLR-FX, Wessling, Germany
[3]Harvard University, Cambridge, MA, USA
[4]JPL, Pasadena, CA, USA
[5]PTB, Braunschweig, Germany
[6]DMT, Boulder, CO, USA
[7]Univ. Mainz, Mainz, Germany
[8]NSF, Arlington, VA, USA
[9]formerly at: FZJ, Jülich, Germany
[a]formerly at: LASP, Boulder, CO, USA

Correspondence to: M. Krämer (m.kraemer@fz-juelich.de)

Abstract

The microphysical and radiative properties of cirrus clouds continue to be beyond understanding and thus still represent one of the largest uncertainties in the prediction of the Earth's climate (IPCC, 2013). Our study aims to provide a guide to cirrus microphysics, which is compiled from an extensive set of model simulations, covering the broad range of atmospheric conditions for cirrus formation and evolution. The model results are portrayed in the same parameter space as field measurements, i.e. in the Ice Water Content-Temperature (IWC-T) parameter space. We validate this cirrus analysis approach by evaluating cirrus data sets from seventeen aircraft campaigns, conducted in the last fifteen years, spending about 94 hrs in cirrus over Europe, Australia, Brazil as well as Southern and Northern America. Altogether, the approach of this study is to track cirrus IWC development with temperature by means of model simulations, compare with observations and then assign, to a certain degree, cirrus microphysics to the observations. Indeed, the field observations show characteristics expected from the simulated cirrus guide. For example, high/low IWCs are found together with high/low ice crystal concentrations N_{ice}.

An important finding from our study is the classification of two types of cirrus with differing formation mechanisms and microphysical properties: the first cirrus type ~~is rather thin with lower IWCs and~~ forms directly as ice (in-situ origin cirrus) and splits in two subclasses, depending on the prevailing strength of the updraft: in slow updrafts these cirrus are rather thin with lower IWCs, while in fast updrafts thicker cirrus with higher IWCs can form. The second type consists predominantly of thick cirrus originating from mixed phase clouds (i.e. via freezing of liquid droplets – liquid origin cirrus), which are completely glaciated while lifting to the cirrus formation temperature region (< 235 K). In the European field campaigns, slow updraft in-situ origin cirrus occur frequently ~~at slow updrafts~~ in low and high pressure systems, ~~but also~~ while fast updraft in-situ cirrus appear in conjunction with ~~faster updrafts~~jet streams or gravity waves. Also, liquid origin cirrus mostly related to warm conveyor belts are found. In the US and tropical campaigns, thick liquid origin cirrus which are formed in large convective systems are detected more frequently.

1 Introduction

The appearance of high altitude cirrus clouds, consisting of pure ice crystals in a cold environment where liquid water no longer exists[1], is not only intriguing but also a research topic for the past hundred years. The impact of cirrus on climate has been studied since the early 1970s. Cox (1971), for example, questioned whether the presence of cirrus clouds tends to warm or cool the Earth's surface and came to the conclusion that tropical cirrus may have a significant warming tendency while mid-latitude cirrus produce a cooling effect. This is consistent with our understanding today, however, the question of the net global effect of cirrus clouds is still not answered definitively. The latest IPCC report (Boucher et al., 2013) states that together, clouds and aerosols continue to contribute the largest uncertainty to estimates and interpretations of the Earth's changing energy budget and that particularly the fundamental details of the microphysical processes of ice clouds are still poorly understood.

A major reason for this continuing uncertainty is the difficulty of measuring the respective key parameters with the required accuracy on fast-flying jet aircraft at high altitudes, as well as from ground-based and space-borne remote sensing platforms. Another problem is that aircraft measurements cannot capture the evolution of the cirrus cloud properties with time, but provide only snapshots of cirrus properties at the thermodynamic conditions encountered. In most cases, the measurements are shown along the flight tracks where they were obtained or as a function of altitude or temperature. Because of this sampling strategy, it is difficult to study cirrus processes from formation to dissipation based on in-situ observations. Instead, statistically-based approaches appear more promising.

The most common parameters that are measured in cirrus clouds – besides the meteorological variables – are ice water content (IWC), ~~number and size of ice crystals (~~ice crystal number (N_{ice}~~and radius R_{ice} or diameter D_{ice}), their shapes and~~), crystal size and shape as well as relative humidity (with respect to ice, RH_{ice}). Sometimes the number and

[1] This is below about 235 K ($-38\,^{\circ}\text{C}$); large ice crystals falling out of cirrus clouds can be observed at higher temperatures as "fall streaks".

properties of ice nucleating particles (IN) and vertical velocity are also measured. Unfortunately, the measurements of ice crystal number and size as well as RH_{ice} have suffered from instrument issues over the last decades (see e.g. Peter et al., 2006; McFarquhar et al., 2011; Korolev et al., 2011, 2013; Krämer et al., 2013) so that interpretations of earlier observations should be made cautiously. Moreover, it is difficult to draw conclusions about the history of ice nucleation and the evolution of microphysical properties from these observations. Nevertheless, there are numerous aircraft and satellite-based observations, as well as modeling studies contributing to the field of cirrus research (e.g. Heymsfield and Iaquinta, 2000; McFarquhar et al., 2000; Sassen and Benson, 2001; Comstock et al., 2002; Heymsfield et al., 2002b, a; Kärcher and Lohmann, 2002; DeMott et al., 2003; Kärcher and Lohmann, 2003; Cziczo et al., 2004; Archuleta et al., 2005; Möhler et al., 2006; Sassen et al., 2008; Gettelman et al., 2010; Hoose and Moehler, 2012; Cziczo et al., 2013)[2].

To help understand the appearance, properties and microphysical processes of cirrus clouds, our study aims to provide a guide to cirrus microphysics in a parameter space easily accessible by field measurements, i.e. in the IWC-Temperature (IWC-T) portrayal. The reason for this choice is that bulk IWC is a very robust parameter under different aspects: IWC is not as sensitive to atmospheric variations as ice crystal numbers. In addition, the measurement of bulk IWC is less complicated than ice crystal measurements and, finally, this study expands our previous work based on IWC observations (Schiller et al., 2008; Krämer et al., 2009; Luebke et al., 2013~~,~~; note also the large IWC database presented by Heymsfield et al., 2013 and the analysis of cirrus observations during the field campaign SPARTICUS by Muhlbauer et al., 2014, see Section 5.5). Our new approach is to track cirrus IWC development with temperature by means of model simulations, compare with observations and then assign cirrus microphysics and formation mechanisms to the observations.

[2]Out of the nearly thousand cirrus studies since 2000, we provide a list here – created using the Web of Science – containing the 10 most cited and the highly cited studies and also 5 most or highly cited ice nucleation and global modeling studies; references contained already in this paper are not considered.

The first pillar of this work is the comprehensive measurements from the multiple field campaigns we have conducted in the last fifteen years with reliable instrumentation where instrument issues are minimized (see Sect. 2). Second, a "Cirrus Guide" is compiled from an extensive set of model simulations (see Sects. 3 and 4), covering the broad range of atmospheric conditions for cirrus formation and evolution. The model results are then portrayed in the IWC-T parameter space and validated by evaluating the data sets from the field campaigns. From the representation of simulated cirrus, we can then assign, to a certain degree, cirrus microphysics, history and the formation mechanism to specific combinations of IWC, N_{ice} and RH_{ice} inside and outside of cirrus as a function of temperature.

In Part 1 of the study, the field measurements as well as the Cirrus Guide simulations are described and the results with respect to cirrus microphysics and possible history are presented (see Sect. 5). Part 2 contains the assignment of the cirrus formation mechanisms to the observations.

2 Cirrus observations

Cirrus clouds were observed during 17 field campaigns performed between 1999 and 2014 over Europe, Africa, Seychelles, Brazil, Australia, USA and Costa Rica. A map of all 104 flights is shown in Fig. 1. The total time spent in cirrus clouds sums up to about 94 h. A summary of the campaigns, location, aircraft and the instrumentation on board the different aircraft is given in Table 1 and in the following sections. A variety of established instruments are used here, which are already well described in the literature. For brevity, here we give only that information necessary for this study and respective references for each instrument.

2.1 Ice water content and humidity measurements

The ice water content (IWC) is derived during most campaigns from the measurements of $\text{H}_2\text{O}_{\text{tot}}$, which is the amount of total water (gas phase + evaporated ice crystals), and $\text{H}_2\text{O}_{\text{gas}}$, the gas phase water amount. IWC is then calculated by using the following Equa-

tion:

$$\mathrm{IWC} = (\mathrm{H_2O_{tot}} - \mathrm{H_2O_{gas}})/E \quad (1)$$

where E is the enhanced volume out of which the ice crystals are sampled in comparison to the sampling volume of the gas phase. For more details see Schiller et al. (2008) and Luebke et al. (2013). H_2O_{tot} was measured by the total water instruments FISH and CLH (Table 1a and b), H_2O_{gas} with the gas phase water instruments FLASH, OJSTER, HWV, JLH, SEAL and SHARC (c–h in Table 1). For details about the instruments see the respective references in the table.

Since no total water measurements were available, IWC for COALESC, ML-CIRRUS and ACRIDICON-CHUVA is derived by integrating the ice crystal size distributions from NIXE-CAPS (see next section) using the mass-dimension (m–D) relation (see Luebke et al., 2015, modified m–D relation of Mitchell et al., 2010):

$$m = a \cdot D^b \quad (2)$$

with

$a = 0.001902, \quad b = 1.802 \quad$ for $\quad D > 240\,\mu\mathrm{m}.$

$a = 0.058000, \quad b = 2.700 \quad$ for $\quad D = 10 - 240\,\mu\mathrm{m}$

ice crystals are spheres $\quad$ for $\quad D < 10\,\mu\mathrm{m}$

In a recent study, Erfani and Mitchell (2015) developed new, observation based m–D relations. These new relations confirm Mitchell et al., 2010 and show that for the cirrus cloud temperature range T < -38°C the m–D relations have nearly no dependence on temperature or cirrus type, thus demonstrating the robustness of the connection between cirrus ice crystal size and mass.

The relative humidity with respect to ice (RH_{ice}; shown in Part 2 of the study) is also derived

from H_2O_{gas} using:

$$RH_{ice} = 100 \cdot \frac{H_2O_{gas}}{H_2O_{sat,\,ice}} \tag{3}$$

where $H_2O_{sat,\,ice}$ is a function of temperature (Murphy and Koop, 2005). The accuracy of the water vapor instruments was debated during the last decade and thus a couple of studies were carried out to investigate their performance under laboratory and field conditions. The good agreement of the instruments deployed in the field campaigns investigated here is stated by the studies of Fahey et al. (2014); Rollins et al. (2014); Meyer et al. (2015). These studies provide further details of this group of instruments. Together with the respective uncertainties of the temperature measurements, the accuracy of the RH_{ice} observations here is between 10 and 20 %.

2.2 Ice crystal measurements

Ice crystal number (N_{ice}) size distributions were measured during the different campaigns by the cloud spectrometers

FSSP-100/300	$D_{ice} = 3$–$30\,\mu m$
CAPS	$D_{ice} = 3$–$930\,\mu m$
NIXE-CAPS	$D_{ice} = 3$–$930\,\mu m$
2D-S	$D_{ice} = 15$–$1280\,\mu m$

D_{ice} denotes the instruments cloud particle size ranges used for this study, although the respective ranges might be larger (see Table 1 i–m and respective references). The upper size limits of the instruments differ. However, the largest contribution to the total ice crystal concentration comes from sizes between 3 and about 30 µm; the concentrations of larger ice particles is in general about three orders of magnitude lower. Hence, the total ice number is covered by most instruments. The 2D-S with the smallest size at 15 µm does not record the smallest ice crystals, whose contribution to the total ice crystal number is highly variable

and depends on cloud age: in the early stage of a cirrus most of the ice crystals are small, but grow to larger sizes when the cirrus develops.

The quality of cloud spectrometer measurements is – as with humidity – under ongoing discussion. In particular, a boost of smaller ice crystals appearing through shattering of large crystals at the instrument tips was discovered as a source of error in many older observations (see e.g. Krämer et al., 2013, and references therein).

Out of the instruments used here, FSSP-100/300 and CAS during MidCix 2004 (part of the CAPS = CAS + CIP[3]) might be affected by shattering, since at that time the particles interarrival times could be recorded only with CIP, but not with CAS. To eliminate shattering artifacts, the data set from the CAPS instrument is carefully re-processed for this study by adjusting the size distributions in the overlap range of the two instruments to each other. This was necessary for this campaign since very large cloud particles, up to the CAPS upper size limit 930 µm, were often present. However, it cannot be ruled out that some shattering influence is still present in the MidCix ice crystal data set, especially since there is an offset in the N_{ice} measurements in comparison to the other campaigns, which might represent either stronger ice nucleation in faster updrafts or shattering. Nevertheless, taking this offset into account, the MidCix data are a valuable contribution when looking at relative changes of ice crystal concentrations.

A contamination of the measurements from FSSP-100/300 by shattered ice crystals was discussed by Krämer et al. (2009), who stated that a significant effect from shattering is not expected at low temperatures where the ice crystals are smaller, but only at temperatures where the occurrence of larger ice crystals increases. From the analysis of the full data set of this study together with the cirrus simulations we can now conclude that during the campaigns where the FSSP-100/300 were deployed, the ice crystals were not as large as during MidCix or MACPEX, and the ice crystal numbers do not exceed the possible atmospheric range as during those WB-57 campaigns where ice crystal shattering became

[3]Two instruments are integrated in the CAPS (Cloud and Aerosol Particle Spectrometer): (1) CAS (Cloud and Aerosol Spectrometer: 0.6–50 µm) and (2) CIP (Cloud Imaging Probe, CIP:15-930 µm), (Baumgardner et al., 2001).

obvious (e.g. CRYSTAL FACE). Hence, though shattering cannot completely be ruled out, the ice crystal numbers appear to be dominated by natural ice production processes. Thus, we believe that the ice crystal number data set from the Geophysica/Learjet – campaigns is suitable for the study presented here.

The 2D-S (MACPEX 2011) is a new generation cloud instrument, which is equipped with tips and software to minimize shattering effects. However, it starts to record ice crystals at larger sizes than the other instruments (15 µm in comparison to 3 µm, see above; note that technically it starts recording at 5 µm, but it is recommended not to use the size bin between 5–15 µm) and thus the total ice crystal number is lower. Nevertheless, as for the MidCix CAPS data, taking this offset into account, the MACPEX data provide a valuable contribution when looking at relative changes of ice crystal concentrations.

The CIP (part of CAPS used for TC-4) as well as NIXE-CAPS (ML-CIRRUS 2014) are also new generation cloud instruments so there are no restrictions for these data sets. NIXE-CAPS is a further development of the CAPS instrument, the new features and data evaluation procedure are described in Meyer (2012) and Luebke et al. (2015). One improvement realized for NIXE-CAPS is is a modification of the particle inlet of the CAS probe – which is part of NIXE-CAPS – to minimize shattering. The wall of the inlet entrance is now "knife edged", greatly reducing the area susceptible for ice crystal shattering. Comparisons to particle size and concentration measurements using other instruments such as SMPS, APS, VIPS, SID-3, 2D-S, CPD, made at the cloud chamber AIDA and on aircraft yield good agreement between the probes (Meyer, 2012).

2.3 Field measurements of IWC and N_{ice}

The total IWC database from all campaigns shown in Table 1 and Fig. 1 is presented in Fig. 2 as a function of temperature (left panel: mixing ratio, right panel: concentration). Altogether, about 94 hrs of flight time was spent in cirrus clouds, thus considerably extending the IWC climatologies of Schiller et al. (2008) (27 hrs) and Luebke et al. (2013) (38 hrs). Nevertheless, the median and core IWC – functions derived by Schiller et al. (2008) and confirmed by Luebke et al. (2013) are also valid for the new, extended IWC climatology.

In Fig. 3 the IWC measured during the individual field campaigns are shown. The color code is the ice crystal number N_{ice}. The time of the simultaneous measurements of IWC and N_{ice} is indicated in the panels and sums up to 85.7 hrs for all campaigns, a little ~~lesser~~ less than the 94 hrs quoted earlier because of the ~~lesser~~ reduced overall sampling time of N_{ice}. In the lower left panel, the part of the IWC climatology of Schiller et al. (2008) where IWC and N_{ice} ice particle measurements were performed simultaneously is shown. Simultaneous IWC and N_{ice} measurements from TC-4 and MidCix are part of the climatology of Luebke et al. (2013) and are here shown in the right column. Recent studies are MACPEX, COALESC, AIRTOSS-ICE, ML-CIRRUS and ACRIDICON-CHUVA. The quite different ranges of IWC and the distribution of N_{ice} within these ranges will be discussed by comparing the measurements with a simulated cirrus climatology (Cirrus Guide, Sects. 5.1 and 5.2) in Sect. 5.3.

3 Cirrus simulations

A simulated cirrus climatology (the Cirrus Guide) is compiled by means of the detailed microphysical box model MAID (Model for aerosol and ice dynamics, Bunz et al., 2008; Rolf et al., 2012), which can be operated along idealized or realistic atmospheric air parcel trajectories.

3.1 MAID

MAID simulates ~~ice clouds that~~ parcels of ice clouds where the ice crystals form directly from the gas phase in the temperature range below about 235 K. The ice nucleation processes implemented in MAID are heterogeneous freezing after Kärcher et al. (2006) and homogeneous freezing after Koop et al. (2000). The heterogeneously freezing ice nuclei (IN) can vary in concentration as well as freezing threshold (RH_{ice}, see Fig. 4): RH_{ice}^{MD} represents very efficient IN with a low freezing threshold (MD: mineral dust), while RH_{ice}^{CS} (CS: coated soot) are quite inefficient IN having a high freezing threshold (Gensch et al., 2008). The homogeneously freezing aerosol particles are assumed to be supercooled binary so-

lution particles with a concentration of 300 cm^{-3} and a mode size of 200 nm. The threshold for homogeneous ice nucleation is higher than that of heterogeneous freezing (see Fig. 4, middle). Thus, in the case where both IN and supercooled solution particles are present, heterogeneous freezing occurs first.

Once the ice particles have formed at the water activity where the ice nucleates, they grow by diffusional growth in separate size bins (Lagrangian ice particle tracking). When the temperature becomes warmer and the air parcel subsaturates, the ice crystals sublimate and return their water vapor to the air parcel.

Ice crystal sedimentation is treated in MAID following the sedimentation scheme of Spichtinger and Gierens (2009), which uses ice mass and number-weighted terminal velocities (after Heymsfield and Iaquinta, 2000) to simulate sedimentation of ice crystals. The ice flux through the model box is defined by the "sedimentation factor" (sedi-f) and represents the ratio of the flux through the top divided by the flux through the bottom. sedi-f $= 0$ means there is no flux from above into the model box and all ice particles will fall out through the bottom (cloud top), sedi-f $= 1$ represents the cloud bottom where the flux from above is equal to the downward flux from the bottom, which simulates a no sedimentation scenario.

The trajectory parcel simulations do not capture dynamical processes such as shear, entrainment, and cloud radiation-dynamics interactions, which might reduce the ice number concentrations below the initial values obtained by nucleation Dinh et al. (2014).

3.2 Cirrus scenarios

In one MAID Cirrus Guide scenario the cirrus temperature space is scanned in 10 K steps between 190–230 K (see Fig. 4, left). For each of the five temperatures, simulations with constant vertical velocities of 0.01, 0.1, 0.5, 1.0, 3.0 $m\,s^{-1}$ are performed, which are initialized with a water amount of 90 % RH_{ice} (T). This sums up to twenty five simulations. Further, as at 190 and 200 K the vertical velocity of 0.001 $m\,s^{-1}$ is added to enclose the range of large scale upward motions at the cold temperatures in the Tropical Transition Layer (TTL). Altogether, one scenario contains 27 simulations. They represent the formation and evolution of cirrus clouds during air parcel ascent, covering the atmospheric range from slow

frontal large scale updrafts up to fast lifting in jetstreams or convection. The sublimation phase of the clouds is not considered in the simulations. Also, ice crystals sedimenting into subsaturated air as e.g. fall streaks are not included in the simulations.

For the complete MAID Cirrus Guide, 36 scenarios (972 model runs) were performed altogether, each varying in the initial and boundary conditions. First of all, pure homogeneous freezing (HOM) or heterogeneous followed by homogeneous freezing (HET + HOM) is allowed to occur. Second, the temperature course of the trajectory can be chosen to be a constant updraft or the updraft can be superimposed with temperature fluctuations. Further, the IN number and freezing threshold and the sedimentation parameter are prescribed for each scenario (see Fig. 4, right).

For the constant updrafts, two HOM scenarios with varying sedi-f (0.9 and 0.5: moderate and strong ice particle sedimentation) are performed, while for HET + HOM 16 scenarios are realized for each combination of: four possible IN numbers (0.001, 0.01, 0.1, 1.0 cm^{-3}: very low to very high), two different freezing thresholds (MD, CS) and two sedimentation parameters (sedi-f $= 0.9$, 0.5). That means that each constant updraft scenario is simulated 18 times under different conditions, summing up to a total of 486 model runs. The scenarios are abbreviated as follows: the 16 HET + HOM scenarios are $\mathrm{HET} + \mathrm{HOM}|_{\text{sedi-f}}^{\text{IN-MD/CS}}$, the two pure homogeneous freezing scenarios: $\mathrm{HOM}|_{\text{sedi-f}}$.

Finally, the 18 scenarios are repeated by superimposing temperature fluctuations on the constant vertical velocities. The fluctuations are superimposed with five different frequencies (2×10^{-4}, 8×10^{-4}, 2×10^{-3}, 4×10^{-3}, 8×10^{-3} Hz) to cover those fluctuations significant for cirrus formation and to reproduce the typical turbulence spectrum found in the atmosphere. The amplitudes are statistically distributed, whereas the maximum amplitudes increases with height and range from 0.3 K for the slowest constant vertical velocity to 4 K for the fastest constant vertical velocity. The frequency spectra and the resulting power spectral density (PSD) are in accordance with Kienast-Sjögren et al. (2015) and also with in-situ measurements of temperature fluctuations during several aircraft campaigns (e.g. MACPEX, see Jensen et al., 2013b).

We would also like to mention that the computer time needed for the complete MAID Cirrus Guide sums up to several weeks where multiple PCs are operated simultaneously. The reason is the exact partitioning of the water vapor between gas and solid phase using the different water vapor partial pressures.

4 Cirrus Guide: microphysical properties

4.1 A selected cirrus scenario

As an example, Fig. 5 shows the Cirrus Guide scenario $\mathrm{HET} + \mathrm{HOM}|^{0.01-\mathrm{MD}}_{\mathrm{sedi}-0.9}$, which we consider as the "middle case" with assumed mean IN conditions of $0.01\,\mathrm{cm}^{-3}$, MD, and a moderate sedimentation of sedi-f $= 0.9$[4]. In the 2nd panel (from top to bottom) IWC is plotted vs. temperature in the same way as the observations shown in Fig. 2. The 3rd/top panels show the respective ice crystal numbers N_{ice} / mean mass radii (R_{ice}) together with minimum, middle and maximum $N_{\mathrm{ice}}/R_{\mathrm{ice}}$ lines derived by Krämer et al. (2009) from observations[5]. The $\mathrm{RH}_{\mathrm{ice}}$ development of the scenarios is shown in the bottom panel, together with the saturation line and the homogeneous freezing threshold. The simulations run from right to left in the figure (indicated by the arrow), starting at the highest temperature and cool further with the respective vertical velocity. The simulation time with temperature is indicated in the legend (in $\mathrm{min\,K}^{-1}$).

The first impression from Fig. 5 is that the simulated IWC climatology is well within the bounds of the observations (see Fig. 3). $\mathrm{RH}_{\mathrm{ice}}$ ranges between saturation and the homogeneous freezing threshold as expected (subsaturation is not expected here since the simulations represent the cooling phase of the cirrus and evaporation was not considered).

[4]Here and in the rest of our study we present the results of our simulations with constant updraft ("nofluct"), since the cirrus evolution can be seen more clearly in these scenarios. In Sect. 4.3 it is shown that the general cirrus patterns are well represented by the "nofluct" simulations.

[5]The mean mass radius $R_{\mathrm{ice}} = \mathrm{IWC}/N_{\mathrm{ice}}$ is used for the representation of the model results for particle size, because it is comparable to the established cloud effective radius R_{eff}.

However, N_{ice} exceeds the range of observations for fast updrafts and falls below for slow updrafts. For all scenarios (including those not shown here), N_{ice} does not change in fast updrafts but varies more in slow updrafts.

A reason that the high N_{ice} are above the maximum line of the observations is that the fast updrafts producing thick cirrus clouds with many ice crystals have a lifetime on the order of only minutes. They may live longer in multiple repeated cycles, such as in case where they are formed in stationary waves like leewave cirrus downstream of mountains. Nevertheless they are small scale phenomena and thus there is a low probability that they will be sampled by aircraft, unless deliberately targeted, and might not be present in the in-situ data sets. In the TTL, where gravity waves caused by convection from below might produce a larger number of ice crystals, the ice nucleation is stalled since the waves are so short that the updraft is reversed before all ice crystals are produced (see also Spichtinger and Krämer, 2013; Dinh et al., 2016).

N_{ice} below the minimum line do exist, the minimum line derived by Krämer et al. (2009) represents the lower detection limit of the older instruments (FSSP with time resolution of 2 s). These lines are under revision based on more observations with advanced cloud probes.

The second important message from Fig. 5, representative for all scenarios of the Cirrus Guide, is that the simulations can generally be grouped by vertical velocities: red, purple and turquoise (fast updraft) on the one hand, and blue, green and gray (slow updraft) on the other hand. The first group of scenarios achieve high IWCs, high N_{ice} and rapidly decreasing RH_{ice} after ice nucleation, while the second group is characterized by low IWC and N_{ice} but higher RH_{ice}. A more detailed look into cirrus microphysics in the temperature parameter space is given in the next section.

4.2 Cirrus microphysics along selected trajectories

To provide a better understanding and a clearer view of cirrus microphysics in the temperature parameter space, some trajectories of cirrus formation and development are selected from Fig. 5 and are shown in Fig. 6. Since the cloud processes are much more depen-

dent on updraft than on temperature, we discuss two trajectories at slower updrafts (green line: 1 cm s^{-1} at 230 K and blue line: 10 cm s^{-1} at 220 K), three at higher (turquoise, purple and red: 0.5, 1, 3 m s^{-1} at 210 K) and one at a very low vertical velocity representative of the large scale ascent in the TTL (0.01 cm s^{-1} at 190 K). The trajectory time proceeds from higher to lower temperatures, as marked by the black arrow. Note here that the times of the scenarios greatly differ: to cool the air by 1 K, 170/17/0.6 min are needed by the green/blue/red air parcels (low/middle/high updrafts). It should be kept in mind that the trajectories apply to the ice nucleation zone of cirrus clouds and not to regions that sedimenting ice crystals fall into. We discuss the two groups of scenarios – slow and fast updraft cirrus – mentioned in Sect. 4.1.

4.2.1 Slow updraft cirrus

The green trajectory represents large-scale, very slow liftings associated with a large coverage of longer lived cirrus occurring e.g. in low or high pressure systems. Detailed inspection of the development of such cirrus, starting at the highest temperature at 90 % RH_{ice} (Fig. 6, bottom panel) show that when the temperature decreases, RH_{ice} starts to rise up to the heterogeneous freezing threshold. At this point, heterogeneously formed ice crystals (3rd panel) together with a low IWC (2nd panel) appear. RH_{ice} starts to decrease with decreasing temperature since the ice crystals grow by the uptake of water vapor. When the ice crystals reach a size large enough to fall out of the air parcel, N_{ice} and IWC strongly decreases again while RH_{ice} increases simultaneously due to the decrease in surfaces for water uptake. In this case, the cirrus completely vanishes and thus allowing RH_{ice} to steadily increase up to the homogeneous freezing threshold where a second, new ice nucleation event occurs. At the very low updraft speed and high cirrus temperature, the number of ice crystals produced by homogeneous freezing is slightly lower than the number of the heterogeneously formed ice particles of the previous cirrus event (note that in the "fluct" scenarios the homogeneously formed N_{ice} increase slightly due to the superimposed temperature fluctuations). In the remainder of this scenario, as long as the air parcel is cooled, a continuous cycle of ice crystal growth, sedimentation and new homogeneous ice formation proceeds, controlled

by decreasing and increasing RH_{ice}. Notably, during this ongoing sedimentation–ice nucleation cycle RH_{ice} stays at a high level. As soon as the cooling is stopped, RH_{ice} will quickly relax to saturation (not shown here). The lifetime of this cirrus type – very low updraft, very low IWC and N_{ice} – is in the range of hours to days.

The blue lines also show large scale slow updrafts, but a little faster than the green case. The common updraft range of frontal systems is bounded between these two lines (compare blue and green lines at the different temperatures in Fig. 5). Here, RH_{ice} also rises until the heterogeneous freezing threshold is reached and the first ice crystals appear. However, no decrease of RH_{ice} caused by depletion of water vapor on the ice surface occurs, but rather the slope of the RH_{ice} increase weakens. This is because the updraft is now so large that the increase of RH_{ice} by cooling overcomes the water depletion by the ice crystals. Thus, the mean mass radius (R_{ice}) of the ice crystals remains smaller than in the green case (see top panel) which is reflected in a weaker sedimentation and higher IWC in the further development of the cirrus. In addition the cirrus does not disappear, but instead a second, homogeneous ice nucleation event occurs – when the freezing threshold is reached – producing somewhat more ice crystals than in the green case due to the larger updraft. Now, the sedimentation–ice nucleation cycle with slightly changing IWC and N_{ice} and high in-cloud RH_{ice} runs as long as the cooling continues. The lifetime of the low updraft, low IWC and N_{ice} cirrus is in the range of several tens of minutes to hours.

4.2.2 Fast updraft cirrus

The turquoise, purple and red trajectories in Fig. 6 illustrate cirrus formed in large updrafts caused e.g. by gravity waves or orographic waves. Those cirrus typically are of small scale and have a short lifetime of less than an hour. An example is mountain wave cirrus, which indeed can be observed over a longer period; however, such a seemingly longer living cirrus represents continously formed short wave cirrus in standing waves ~~. Their development~~ (note here that for such cases our simulations represent one cloud parcel passing the wave). The development of fast updraft cirrus, starting again at the highest temperature of the trajectories at 90 % RH_{ice} ~~in~~ (Fig. 6~~(~~, bottom panel) ~~,~~ is comparable to the other sce-

narios – but much faster – for the first, heterogeneous freezing events. However, then RH_{ice} quickly increases up to the homogeneous freezing threshold and a strong outburst of homogeneously formed ice crystals appear, with more crystals formed the faster the updraft. Thus, the IWC reaches high values, but the crystals remain small since the available water is distributed equally on the many ice particles. As a consequence, sedimentation is of minor importance in such cirrus and the in-cloud RH_{ice} quickly drops down to a dynamical equilibrium close to saturation.

4.2.3 TTL cirrus

Cirrus in the very cold tropical tropopause layer are special. They have very low ice crystal numbers found together with high RH_{ice} (Krämer et al., 2009; Jensen et al., 2013a), but spikes of high ice numbers embedded in saturation are also reported by Jensen et al. (2013a). Case studies of TTL cirrus observations are also analysed by Frey et al. (2011, 2014). Spichtinger and Krämer (2013) and recently Dinh et al. (2016) state that low N_{ice} in high supersaturation are mostly produced by homogeneous freezing in very slow large scale updrafts, superimposed by very short gravity waves. Due to the shortness of the waves, the ice nucleation process is stalled at the beginning when only a few ice crystals have formed. The IWC is accordingly low. In addition, Dinh et al. (2016) explain the high N_{ice} in saturation by small variations of water vapor which cause very high supersaturations during the ice nucleation process and thus many more ice crystals.

Though this cirrus formation mechanism is not included in our simulations, we attempt to form these cirrus by assuming heterogeneous-homogeneous freezing in very slow large scale updrafts (gray case; the IN number is only 0.001 cm^{-3} which is more typical for the TTL). ~~The observations of low~~ Low N_{ice} and IWC together with high RH_{ice} can be reproduced with these assumptions. Note, however, that the sensitivity case simulated here produces lower N_{ice} than the averge concentration of 0.03 cm^{-3} reported by Spichtinger and Krämer (2013).

The evolution of the cirrus is comparable to the green case: the first heterogeneously formed cirrus crystals sediment out and the next cirrus is formed purely homogeneously

since all IN are already consumed. However, the spikes of high ice numbers embedded in saturation could not be explained with this model approach. Nevertheless, from the data set of Krämer et al. (2009) it seems that low N_{ice} are the favored state in TTL cirrus. A conclusion for the representation of TTL cirrus by global models – which in most cases overestimate TTL ice crystal numbers – could be that the approach used here might be an useful approximation.

4.3 A cirrus scenario ensemble

A representative sampling of all 36 cirrus scenarios in the IWC-T parameter space is shown in Fig. 7. Each panel includes all 27 trajectories, covering the full cirrus temperature and vertical velocity range, as described in Sect. 3 (see Fig. 4). Eight scenarios are shown here: the top row represents simulations with efficient IN like mineral dust (MD, low freezing threshold) and the bottom row inefficient IN like coated soot (CS, high freezing threshold), while the columns show varying IN concentrations. For all scenarios shown here the sedimentation factor is assumed to be moderate (sedi-f $= 0.9$).

It is obvious from Fig. 7 that the differences between the IN initial conditions (concentration and freezing threshold) do not greatly influence the general pattern of the IWC-T portrayal of cirrus. In other words, it means that the IWC is a quite stable parameter, particularly in comparison with the variability of N_{ice} and R_{ice} in dependence to the initial atmospheric conditions (see Sect. 5.3, Fig. 12).

In Fig. 8, the scenario $\text{HET} + \text{HOM}|^{0.01-\text{MD}}_{\text{sedi}-0.9}$ (same as in Fig. 7: red box; see also Figs. 5 and 6) is shown three times. The left panel depicts the IWCs when temperature fluctuations are superimposed on the constant vertical velocities ("fluct" runs). It can be seen that the general IWC distribution is preserved, looking less structured, while the individual model runs are generally shorter in comparison to the "nofluct" cases ($=$ constant updrafts). The IWC oscillations are parallel to the temperature course, reflecting growing and shrinking ice crystals with increasing and decreasing temperature. The shorter lifetimes can be explained by the fact that the temperature fluctuations contain warming phases so that the cirrus clouds simply evaporate. From the middle panel ("nofluct" scenario, color coded by time

from blue to red) it can be seen that the parts of the simulations that have disappeared in the "fluct" scenario are cirrus older than about 18 h (reddish colours). Since the general pattern of IWC evolution is more clear in the "nofluct" simulations, we prefer to show those in this study, though the scenarios with temperature fluctuations better reflect atmospheric conditions.

Next, in the right panel of Fig. 8 the scenario "nofluct" is shown again, but with enhanced sedimentation (sedi-f $= 0.5$). Here, a decrease of IWCs can be seen, in particular at warmer temperatures, where the ice crystals are large and preferentially fall out. However, from comparison of the Cirrus Guide scenarios with the meteorological situations found in the observations (see Sect. 5.3), we can conclude that the observations are better represented by the simulations with moderate sedimentation (sedi-f $= 0.9$).

5 Cirrus Guide: cloud types

First of all, we remind the reader that the ice clouds represented in the Cirrus Guide are "in-situ origin cirrus". This means that this type of ice clouds is formed "in-situ" in the temperature range below about 235 K directly from the gas phase. The reason for being so specific will become obvious in the following subsections.

5.1 In-situ origin cirrus in slow and fast updrafts

From the previous sections we conclude that two types are not only found in selected trajectories (Sect. 4.2), but are a general feature of mid-latitude in-situ origin cirrus (205–235 K, Sect. 4.3).

5.1.1 Slow updraft cirrus

The first type is characterized by slow updrafts, producing low-middle IWCs which consist of low-middle N_{ice} with middle-to large R_{ice} (see black solid and dotted lines in Fig. 5). Sedimentation plays a crucial role by controlling the development of microphysical prop-

erties and the in-cloud supersaturation: in the HET part of the "slow updraft cirrus", RH_{ice} lies between the heterogeneous and homogeneous freezing threshold, while in the later HET + HOM part RH_{ice} remains slightly below the homogeneous freezing threshold. The formation mechanism of this cirrus type starts with HET freezing that is followed by a second, HOM ice nucleation event (since all IN are already consumed) if the cooling phase is long enough and temperature fluctuations do not cause a HOM freezing event earlier. Thus, the slow updraft cirrus have a possibility to remain as purely HET formed ice clouds. On the other hand, purely HOM formed cirrus also only appear in the long lasting, slow updraft cirrus: they evolve after the earlier HET cirrus have disappeared by sedimentation. The frequency of occurrence of these cirrus is unknown.

5.1.2 Fast updraft cirrus

The second type are "fast updraft cirrus" with high ice crystal numbers and IWCs. Sedimentation does not play a great role in this cirrus type and thus the in-cloud RH_{ice} quickly reduces to saturation. The formation mechanism of this cirrus type is also HET + HOM, but it is dominated by HOM ice formation.

5.2 Cirrus microphysics in the IWC-T parameter space

We can conclude that cirrus microphysics is visible in the IWC-T parameter space up to a certain degree, i.e. depicting measurements of IWC vs. temperature gives an impression of the nature of observed cirrus without the need of more detailed microphysical measurements. This is summarized in the sketch shown in Fig. 9, where we plotted some of the MAID scenarios together with the median, core and maximum IWC-lines to guide the eye.

IWCs below the median line mostly stem from slow updraft cirrus in low or high pressure systems. They consist of a few, but large ice crystals which are – due to the increasing amount of available water vapor – larger the warmer the cirrus is. The first part of these cirrus is determined by HET freezing. However, if the cloud life time is long enough, HOM freezing will start as well. Due to the slow updrafts, the number of ice crystals produced by

HOM freezing is on the same order of magnitude as the HET nucleated ice crystals and thus also have low IWCs. We emphasize here that in slow updraft regions the difference in microphysics between homogeneous and heterogeneous freezing is small. In this cirrus type, sedimentation plays an important role, controlling the microphysical properties and might produce fallstreaks, which causes some vertical redistribution of water.

High IWCs above the median line are mostly produced by fast updraft cirrus caused by atmospheric waves. The cirrus is only briefly at low IWC during the HET phase since the HOM freezing quickly pushes the IWC above the median line. With their large number of small, non-sedimenting ice crystals, these cirrus are microphysically very different from the slow updraft cirrus.

An impression of the radiative properties in terms of extinction of the two cirrus types is given in the lower right panel of Fig. 12, where the ice crystal number N_{ice} is shown vs. the corresponding mean mass radius R_{ice} for all temperatures. The IWCs are plotted as black isolines. The top panel shows the same, but with color code IWC, in the left panel the color code is vertical velocity. The extinction of all simulated cirrus is calculated from the empirical relationship between IWC and extinction provided by Gayet et al. (2004). Those cirrus with a low number of large crystals (slow updraft, low IWC, see top and left panel) have a small extinction, i.e. they are optically thin, while the cirrus with the many small ice crystals (fast updraft, large IWC, see top and left panel) have larger extinctions and are optically thicker.

The majority of cirrus clouds in the atmosphere are of the first "slow updraft" type, i.e. they appear on a larger scale and have a longer lifetime, while the second "fast updraft" type occurs less frequently since the fast updrafts are limited in space and time (note here that "fast updraft" does not include convection in the simulations; "convective" or "anvil" cirrus will be addressed later in Sections 5.4 and 5.5).

5.3 Comparison of simulations and observations

In this section, we compare observed and simulated cirrus clouds to demonstrate that the simulated Cirrus Guide shown in Fig. 9 is confirmed by measurements and thus is indeed appropriate for an impression of the cirrus microphysics.

5.3.1 IWC-T parameter space

In Fig. 10 (upper left panel) the simulated Cirrus Guide is shown again, but color coded by the ice crystal number N_{ice}. It can be seen that in the simulations few ice crystals are present below the median IWC line (light blue), while more and more (darker blue) N_{ice} appear with increasing IWC. As described in Sect. 3.2, the simulations in the Cirrus Guide represent the formation and evolution of cirrus as long as the air parcels are cooled. Subsaturated environments with shrinking ice crystals or fallstreaks are not included. Thus, there is the possibility that a part of the small IWCs in the observations are not comparable to those simulated in the Cirrus Guide.

From all of our measurements, we have compiled a data set that compares best to the Cirrus Guide (Fig. 11). For that pupose, we used only measurements where $\text{RH}_{\text{ice}} > 95\,\%$. Also, only those campaigns where ice crystals with diameters larger than 3 µm were measured and ice crystal shattering effects are minimized were considered (Geophysica – TTL flights, COALESC, AIRTOSS-ICE, ML-CIRRUS; ACRIDICON 2014 fits these requirements but is not considered since it is nearly entirely driven by strong convection). Comparing Fig. 10 (upper left panel, simulations) with Fig. 11 (observations) yields in general the same N_{ice} pattern in the simulations and the measurements. This means that the simulations are able to represent the increasing ice crystal number with increasing IWC seen in the measurements. Some dots in darker blue colors are visible in the observations, particularly at higher IWC. They can be traced back to situations with higher vertical velocities and thus represent the rare fast updraft cirrus discussed above.

Looking back now at the full data sets of the individual campaigns (Fig. 3), it can be seen that the decreasing N_{ice} with decreasing IWC is visible in all field campaigns, even when the measurements are under suspicion of shattering effects. This suggests that in the respective data sets shown here, the amount of small artifacts of shattered ice crystals is not large enough to overlay the microphysical cirrus properties. Thus, we look now in more detail at the different field experiments.

We start with the AIRTOSS-ICE campaign (Fig. 3, left column, top panel). Here, one can see that very low N_{ice} concentrations were observed. The measurements were performed in August and September 2013 above the German North Sea (for geographical regions see Fig. 1) under Indian summer conditions, which implies that very low vertical updrafts associated with high pressure systems prevailed during the flights.

The IWC climatology from the Geophysica/Learjet measurements between 1999 and 2006, which covers a large geographical range, is shown in Fig. 3 (left column, second panel from top). Measurements in the TTL ($T < 200$ K) are contained here, with very low N_{ice} detected at low IWCs – probably formed in very slow updrafts – but also higher N_{ice} together with high IWCs formed at higher updrafts. These two types of cirrus are also observed during the Global Hawk ATTREX mission in the TTL (Jensen et al., 2013a). Additionally, very high N_{ice} (dark blue points) can be seen above the median IWC line in the measurements at temperatures larger than about 205 K. Closer inspection of the meteorological situation shows that these measurements were performed downstream of the Norwegian mountains at very high vertical velocities and can be interpreted as leewave cirrus. High N_{ice} below the median IWC line in this temperature range might be a result of ice crystal shattering.

Calmer meteorolgical conditions prevailed during COALESC (left column, second panel from bottom) in spring 2011 over the Southern part of the UK. This is visible in the quite smooth color gradient, only disturbed by a dark blue patch at higher IWC between 210 and 215 K. These high ice crystal numbers represent very fresh contrails, which were chased during one flight. The grouping of the points in a small temperature range reflect the cruising altitude of passenger aircraft.

ML-CIRRUS (Fig. 3, left column, bottom panel) took place in spring 2014 over Europe. Here, low and high pressure systems, some jet stream cirrus as well as contrails and aviation induced cirrus were probed. Nevertheless, the pattern of N_{ice} increasing with IWC is also visible here. As during COALESC, a block of higher N_{ice} at higher IWC around 210 K is found, though N_{ice} is a little lower here. They represent older contrails and aviation induced cirrus which were omnipresent in the cirrus probed over Central Europe.

Next, we discuss the two campaigns over the US continent, MACPEX (2011) and MidCix (2006), TC-4 (2007) over Costa Rica and ACRIDICON-CHUVA (2014) over Brazil (Fig. 3, right column). Again, the general pattern of N_{ice} increasing with IWC can clearly be seen in the measurements, though TC-4 is in general on the lower IWC side in comparison to MidCix and MACPEX and especially ACRIDICON-CHUVA, which reaches very high IWCs. The meteorological situations for MidCix and MACPEX, which took place in the same region (Southern US continent), were mostly determined by mesoscale convective systems with high updrafts, while ACRIDION-CHUVA represents smaller scale tropical deep convection.

What is surprising for ML-CIRRUS, MidCix and MACPEX and particularly ACRIDION-CHUVA are the many data points at very high IWCs: high IWCs should appear from fast updrafts, which are discussed as small scale features that do not appear frequently (see Sect. 5.1). To further investigate this, we have plotted the simulated Cirrus Guide again, now color coded by the the mean mass size R_{ice} of the ice crystals in Fig. 10, upper right panel. It is seen that R_{ice} is largest (dark green) at low IWCs and high temperatures. For comparison the same plot type is shown for MidCix in the panel below (for consistency the MidCix IWC colored by N_{ice} is shown in the left panel). Conversely to the simulations, the largest ice crystals appear at the highest IWCs in the MidCix observations. Seemingly, these frequently appearing cirrus with high IWCs and large ice crystals are not present in the simulations of in-situ origin cirrus. They represent a different type of ice clouds originating in liquid droplets, which will be further discussed in Sect. 5.4.

5.3.2 N_{ice}–R_{ice}–IWC parameter space

For the ML-CIRRUS (2014) campaign, it was possible to extract the in-situ origin cirrus from the observations by analyzing the cloud history along backward trajectories (for more detail see Luebke et al., 2015; Rolf et al., 2015). Hence, this data set is particularly suitable for comparison with the MAID simulations. For that purpose, we show a different type of plot (introduced already in Sect. 5.2), including the information of IWC, N_{ice} and R_{ice} all at once. In Fig. 12 the ice crystal number N_{ice} is plotted as function of R_{ice}. In the upper row, the color code is IWC and the black lines are isolines of constant IWC. The upper left

panel shows the observations during ML-CIRRUS (2014) and in the right panel the Cirrus Guide simulations of all "fluct" scenarios (including temperature fluctuations, see Sect. 3) are shown. For a better interpretation, the same plot is shown in the lower left panel of the Figure, now color coded by vertical velocity in the same colors used in previous figures. In the lower right panel the color code is extinction (see Sect. 5.2).

Inspection of the Cirrus Guide vertical velocity plot (Fig. 12, lower left) shows that high updrafts (red dots) can produce ice crystals smaller than 10 µm (mass mean radius) with concentrations between 5–500 cm^{-3}. With decreasing updraft, N_{ice} decreases to values down to 10^{-4} cm^{-3} while R_{ice} grows to maximum sizes of 100 µm. Note that R_{ice} is also an indicator for cirrus age, the larger the mass mean size, the older the cloud. Comparing with the IWC plot (upper right) it can be seen that lower vertical velocities are related to lower IWCs with fewer, larger ice crystals and higher updrafts with higher IWC and more, smaller ice crystals (as also shown in Sect. 5.2).

From a comparison of the observations (upper left) with the simulations (upper right), it is evident that the observed cirrus are located well within the bounds of the simulations. The range of values covered by the observations is smaller because they represent mid-latitude cirrus clouds with temperatures between about 205–235 K and mostly slow updrafts, while the simulations represent the full cirrus climatology including colder temperatures and higher vertical velocities. The observed concentrations of small ice crystals 5–20 cm^{-3} are mostly related to the contrails noted already in the previous section. Also, some meteorological situations with higher updrafts were probed during the campaign, leading to observations with a maximum N_{ice} of 5 cm^{-3}. The maximum sizes of the observed cirrus particles are smaller than in the simulations, which points to a shorter cirrus lifetime in the atmosphere than in the simulations. Also, some thicker cirrus (red points between the IWC isolines 200–300 ppmv) are detected during ML-Cirrus. However, given the wide range of different parameters influencing the cirrus formation and evolution, the good agreement between observations and simulations demonstrates that with the help of the Cirrus Guide an interpretation of cirrus observations is possible in greater depth.

5.4 Liquid origin cirrus

In the last paragraph of Sect. 5.3.1 it is mentioned that high IWCs above the median IWC together with large ice crystals (Fig. 10) are not represented in the Cirrus Guide. Nevertheless, this type of cirrus is found in the observations, especially during MidCix, MACPEX and ACRIDICON-CHUVA, as well as in the other campaigns shown in Fig. 3 (except AIRTOSS-ICE). Here, a larger number of very high IWC are detected than was expected based on the MAID simulations. From further analysis, relating meteorological situations to cirrus types, it can be concluded that these high IWC cirrus stem from lower altitudes and are not produced by in-situ ice nucleation directly from the gas phase like in our simulations (for detail see Luebke et al., 2015). Instead, they are formed by heterogeneous freezing of liquid droplets at temperatures > 235 K or possibly as low as 235 K by homogeneous drop freezing. The ice crystals were then lifted to the temperature range < 235 K and are therefore regarded as cirrus clouds. This can happen in regions with mesoscale convective activity (observed during MidCix and MACPEX), but also in warm conveyor belts (observed during ML-CIRRUS). In tropical convective systems, which are observed in this study during ACRIDICON-CUVA, this cirrus type is known as “anvil cirrus” or “anvil outflow”.

Note that in addition to a high IWC, other indicators for cirrus originating from liquid drops are high N_{ice} together with the appearance of larger ice crystals (for more detail see Luebke et al., 2015). The high ice crystal concentrations may stem from an originally larger frozen drop number, or from an additional freezing event that may happen on top of the preexisting ice in case the updraft is fast enough. The nucleation mechanism will probably be homogeneous freezing, since the IN are already consumed in the previous liquid cloud. The high supersaturation that is needed can be reached in fast updrafts, when the reduction of RH_{ice} by uptake of water on the ice surfaces is less than the RH_{ice} enhancement caused by the decreasing temperature.

Altogether, these thick liquid origin cirrus have microphysical, and thus optical, properties quite different from the in-situ cirrus formed directly via the gas phase. Further, they appear together with mixed-phase and often liquid clouds below. This is shown in detail for liquid

origin clouds stemming from warm conveyor belts in comparison to in-situ cirrus observed during ML-CIRRUS by Luebke et al. (2015).

It is a surprising result from this study that these “liquid origin cirrus” seem to appear in the complete cirrus temperature range with a non-negligible frequency. As a consequence, for a complete understanding we recommend devoting further research to assessing their propertiers and including them in model studies.

5.5 Comparison with other cirrus classifications

Cirrus cloud classifications already exist and are used in the wide literature mentioned in the introduction. Here we intend to compare our findings of the two in-situ origin types and the liquid origin cirrus with the present classifications.

’In-situ’, ’synoptic’ and also ’lee wave’, ’gravity wave’ or ’orographic’ cirrus are used as definitions for cirrus cloud forming directly from the gas phase. Since ’in-situ’ is the most common name -and ’lee/gravity wave’ and ’orographic’ cirrus are already very specific- we followed this approach in our classification. On the other hand, the term ’convective’ or ’anvil’ cirrus is used to classify cirrus clouds representing glaciated, but originally liquid clouds lifted to the cirrus emperature regime in the prevailing updraft. Here, we name this type ’liquid origin cirrus’, since we found that the lifting of clouds to temperatures T $<$ -38°C happens not only in convective systems connected to anvils, but also in warm conveyor belts, in mesoscale convective systems and even in gravity wave clouds.

Thus, compared to the grouping based on specific meteorological situations, the cirrus classification scheme we present here is based on (i) the formation mechanism (directly ice or frozen liquid droplets), which is tied to the temperature threshold of -38°C below which liquid water does not exist, and, (ii) the vertical velocity, which determines the thickness of the cirrus.

A thorough study on the impact of large-scale dynamics on the microphysical properties of midlatitude cirrus has been performed by Muhlbauer et al. 2014. The study is based on cirrus cloud observations during the field campaign SPARTICUS in 2010 in the vicinity of the

ARM SGP site (Atmospheric Radiation Measurement, Southern Great Plains) and analysis of atmospheric states using a combination of ECMWF ERA-Interim reanalysis data with continuous observations from a millimeter-wavelength cloud radar. Four cirrus types are defined by Muhlbauer et al. 2014: (a) ridge-crest, (b) frontal, (c) subtropical jet stream and (d) anvil. Striking differences in the cirrus microphysics (IWC and N_{ice}) for different large-scale environments were found in this study. The authors suggest that vertical velocities are a poor predictor for explaining the microphysical variability in cirrus.

Before comparing the findings of Muhlbauer et al. 2014 with this study, we like to note a difference in the observed IWC ranges: here, IWCs between about 0.001 and $\approx$ 300 mg/m^3 are detected in the SPARTICUS temperature range $>$210 K (see Figure 2, right panel), while in Muhlbauer et al. 2014 the observed range spans from 1 to $\approx$ 400 mg/m^3 (their Figure 6). From Figure 2 (right panel) it becomes obvious that the in-situ cirrus in slow updrafts with low IWCs (in general $<$ 1mg/m^3 , i.e. below the median IWC line) are barely included in the SPARTICUS observations. Thus, the definitions of 'low' and 'high' IWCs differ between the two studies: the peaks of the frequency distributions of ridge-crest cirrus are discussed as low IWC ($\approx$ 8 mg/m^3) in connection with high N_{ice} ($\approx$ 0.2 cm^{-3}) by Muhlbauer et al. 2014. However, in the parameter space of the Cirrus Guide, 8 mg/m^3 is well into the high IWC range, so the classificatoin would be high IWC and high N_{ice}. Frontal and subtropical jet stream cirrus, which are described by Muhlbauer et al. 2014 to have middle IWC and N_{ice} are also in the range of high IWC N_{ice} in the context here. Anvil cirrus have high IWC and N_{ice} in both studies.

Taking this into account, we can relate (a) ridge-crest to fast updraft in-situ origin cirrus - a type of cirrus that is quite rarely found in our observations and (b) frontal cirrus most probably to liquid origin cirrus in slower frontal updrafts (like WCBs in our study). Subtropical jet stream cirrus (c) also seem to be of liquid origin -because of the higher IWCs- with a possible subsequent weak in-situ homogeneous freezing event, and, (d) anvil cirrus are classified as liquid origin in fast updrafts. With respect to a vertical velocity classification, we think that the lack of significant differences detected by Muhlbauer et al. 2014 between the cirrus types is a consequence of observing cirrus classes that are all situated in the fast

updraft range above the IWC median. The slow updraft in-situ cirrus classified in this study exhibit IWCs below the median IWC line and are not included in Muhlbauer et al. 2014.

Altogether, the four classifications provided by Muhlbauer et al. 2014 for the high IWC range agree very well with the cirrus classes of this study. They are more specific than the two types provided here (fast updraft in-situ or liquid origin cirrus), which we have not further specified due to a lack of observations of fast updraft in-situ cirrus. From the few observations we have, we can confirm that fast updraft in-situ cirrus (ridge crest in Muhlbauer et al., 2014) have a lower IWC but higher N_{ice} than liquid origin cirrus (frontal, subtropical jet stream and anvil cirrus in Muhlbauer et al., 2014).

6 Summary and conclusions

The goal of this study is to track cirrus IWC development with temperature by means of model simulations, compare the simulations with observations in the IWC-T parameter space and then assign, to a certain degree, cirrus microphysics to the observations.

To this end, an extensive set of model simulations, covering the broad range of atmospheric conditions for cirrus formation and evolution, is compiled, which we call the Cirrus Guide. Further, cirrus data sets from seventeen aircraft campaigns, conducted between 1999–2014, spending about 94 hrs in cirrus over Europe, Australia, Brazil as well as Southern and Northern America are evaluated.

We found good agreement between observations and simulations, demonstrating that the Cirrus Guide is applicable for the interpretation of observations. A summary of the findings with respect to cirrus microphysics is provided in a sketch of the IWC-T parameter space shown in Fig. 13.

1. Two different types of cirrus are characterized in our study. The first represents the "classical" cirrus (simulated in the Cirrus Guide), where the ice crystals form heterogeneously+homogeneously directly from the gas phase ("in-situ origin cirrus", greenish color in Fig. 13). The second type consists of ice crystals formed by heterogeneous (or sometimes homogeneous) freezing of liquid drops farther below in the atmosphere

which are uplifted into the cirrus temperature range ("liquid origin cirrus", blueish color in Fig. 13). The liquid origin cirrus are not included in our simulations, but are identified from the observations. These two cirrus types in general can be distinguished by IWC, where in-situ cirrus are preferably thin with lower IWC, while liquid origin cirrus are mostly thick with higher IWC. In addition, the liquid origin cirrus seems to have larger ice crystals than the in-situ cirrus. The microphysical properties of the two cirrus types are further investigated by Luebke et al. (2015).

2. Within the in-situ cirrus, two classes are also identified. (1) The first are thin cirrus that appear in slow updraft situations (range up to about 0.1 $\mathrm{m\,s^{-1}}$). Their IWC is low and they consist of few, large ice crystals. Due to the slow updraft, their microphysical properties are only slightly dependent on the type of ice nucleation (heterogeneous or homogeneous). They appear in low or high pressure frontal systems and thus have a large geographic coverage and a long lifetime. (2) The second in-situ cirrus class are thick cirrus forming in fast updrafts triggered by jet streams or atmospheric waves (i.e. leewave cirrus). They have high IWCs and many, small ice crystals. Their formation mechanism is dominated by homogeneous freezing, i.e. they are not sensitive to IN properties. The geographic coverage of fast updraft in-situ cirrus is low. In principle they have a short lifetime, unless they do not form continously in standing waves as e.g. orographic cirrus downstream of mountains.

3. Analyzing the cirrus over the European and American continents, we found that over Europe in-situ and liquid origin cirrus in slow updrafts (warm conveyor belts, high pressure systems) are observed most frequently. Over the American continent, liquid origin cirrus in fast updrafts (mesoscale convective systems, tropical convection) were more abundant in the observations.

To conclusively draw a line from cirrus to the Earth's climate, we ~~hypothesize here~~ suggest here -and will further investigate- that on average the physically and optically thinner in-situ slow updraft cirrus cause a warming effect, while ~~cooling might rather be induced by~~

~~the thicker~~ only thick fast updraft in-situ and particularly thick liquid origin cirrus have the potential to cool.

Acknowledgements. The authors thank the coordinators (listed below) and all teams which were engaged in the field experiments compiled in the study presented here. Progress in the challenging task to understand cirrus clouds and their formation mechanism for most atmospheric conditions was only possible due to the large effort flowing into all the experiments. We also thank Paul Lawson for providing 2D-S data from the MACPEX campaign. Funding is partly provided by the DFG HALO-SPP project ACIS (KR 2957/1-1). Campaign coordinators: APE-THESEO 1999 (Bruno Carli + Kees Blom), ENVISAT 2002 (Kees Blom), EUPLEX 2003 (Fred Stroh + Hans Schlager), ENVISAT 2003 (Kees Blom), TROCCINOX 2005 (Ulrich Schumann + Hans Schlager), SCOUT-O3 2005 (Cornelius Schiller), AMMA 2006: (Kathy Law + Francesco Cairo), MidCix 2004 (Gerald Mace + Andy Heymsfield), TC-4 2007 (Brian Toon), MACPEX 2011 (Eric Jensen + Gerald Mace), COALESC 2011 (Phil Brown), AIRTOSS 2013 (Manfred Wendisch, Peter Spichtinger + Stephan Borrmann), ML-CIRRUS 2014 (Christiane Voigt, Andreas Minkin + Ulrich Schumann), ACRIDICON 2014 (Manfred Wendisch, Uli Pöschl, Meinrad Andreae + Luiz Machado), ATTREX 2014 (Eric Jensen + Leonhard Pfister). Thank unknowingly to the author's of HG2G for inspiring the titel.

The article processing charges for this open-access publication were covered by a Research Centre of the Helmholtz Association.

References

Archuleta, C. M., DeMott, P. J., and Kreidenweis, S. M.: Ice nucleation by surrogates for atmospheric mineral dust and mineral dust/sulfate particles at cirrus temperatures, Atmos. Chem. Phys., 5, 2617–2634, doi:10.5194/acp-5-2617-2005, 2005.

Baumgardner, D., Jonsson, H., Dawson, W., O'Connor, D., and Newton, R.: The cloud, aerosol and precipitation spectrometer (CAPS): a new instrument for cloud investigations, Atmos. Res., 59–60, 251–264, 2001.

Boucher, O., Randall, D., Artaxo, P., Bretherton, C., Feingold, G., Forster, P., Kerminen, V.-M., Kondo, Y., Liao, H., Lohmann, U., Rasch, P., Satheesh, S., Sherwood, S., Stevens, B., and Zhang, X.: Clouds and aerosols, in: Climate Change 2013: the Physical Science Basis. Contribution of Working Group I to the Fifth Assessment Report of the Intergovernmental Panel on

Climate Change, Cambridge University Press, Cambridge, UK, New York, NY, USA, 571–658, 2013.

Buchholz, B., Kühnreich, B., Smit, H. G. J., and Ebert, V.: Validation of an extractive, airborne, compact TDL spectrometer for atmospheric humidity sensing by blind intercomparison, Appl. Phys. B-Lasers O., 110, 249–262, 2013.

Bunz, H., Benz, S., Gensch, I., and Krämer, M.: MAID: a model to simulate UT/LS aerosols and ice clouds, Environ. Res. Lett., 3, 035001, doi:10.1088/1748-9326/3/3/035001, 2008.

Comstock, J. M., Ackerman, T. P., and Mace, G. G.: Ground-based lidar and radar remote sensing of tropical cirrus clouds at Nauru Island: cloud statistics and radiative impacts, J. Geophys. Res., 107, 1–4, 2002.

Cox, S.: Cirrus clouds and climate, J. Atmos. Sci., 28, 1513–1515, 1971.

Cziczo, D., Murphy, D., Hudson, P., and Thomson, D. S.: Single particle measurements of the chemical composition of cirrus ice residue during CRYSTAL-FACE, J. Geophys. Res., 109, D04201, doi:10.1029/2003JD004032, 2004.

Cziczo, D. J., Froyd, K. D., Hoose, C., Jensen, E. J., Diao, M., Zondlo, M. A., Smith, J. B., Twohy, C. H., and Murphy, D. M.: Clarifying the dominant sources and mechanisms of cirrus cloud formation, Science, 40, 1320–1324, 2013.

DeMott, P. J., Cziczo, D., Prenni, A., Murphy, D., Kreidenweis, S., Thomson, D., Borys, R., and Rogers, D.: Measurements of the concentration and composition of nuclei for cirrus formation, P. Natl. Acad. Sci. USA, 100, 14655–14660, 2003.

Dinh, T., Fueglistaler, S., Durran, D. and Ackerman, T.: Cirrus and water vapour transport in the tropical tropopause layer – Part 2: Roles of ice nucleation and sedimentation, cloud dynamics, and moisture conditions. Atmos. Chem. Phys., 14, 12225–12236, doi:10.5194/acp-14-12225-2014, 2014.

Dinh, T., Podglajen, A., Hertzog, A., Legras, B., and Plougonven, R.: Effect of gravity wave temperature fluctuations on homogeneous ice nucleation in the tropical tropopause layer, Atmos. Chem. Phys., 16, 35-46, doi:10.5194/acp-16-35-2016, 2016

Erfani, E. and Mitchell, D. L.: Developing and bounding ice particle mass- and area-dimension expressions for use in atmospheric models and remote sensing, Atmos. Chem. Phys. Discuss., 15, 8771–879928517-28573, doi:10.5194/acpd-15-28517-2015, 2015.

Fahey, D. W., Gao, R.-S., Möhler, O., Saathoff, H., Schiller, C., Ebert, V., Krämer, M., Peter, T., Amarouche, N., Avallone, L. M., Bauer, R., Bozóki, Z., Christensen, L. E., Davis, S. M., Durry, G., Dyroff, C., Herman, R. L., Hunsmann, S., Khaykin, S. M., Mackrodt, P., Meyer, J., Smith, J. B.,

Spelten, N., Troy, R. F., Vömel, H., Wagner, S., and Wienhold, F. G.: The AquaVIT-1 intercomparison of atmospheric water vapor measurement techniques, Atmos. Meas. Tech., 7, 3177–3213, doi:10.5194/amt-7-3177-2014, 2014.

Finger, F., Werner, F., Klingebiel, M., Ehrlich, A., Jäkel, E., Voigt, M., Borrmann, S., Spichtinger, P., and Wendisch, M.: Spectral optical layer properties of cirrus from collocated airborne measurements – a feasibility study, Atmos. Chem. Phys. Discuss., 15, 19045–19077, doi:10.5194/acpd-15-19045-2015, 2015.

Frey, W., Borrmann, S., Kunkel, D., Weigel, R., de Reus, M., Schlager, H., Roiger, A., Voigt, C., Hoor, P., Curtius, J., Krämer, M., Schiller, C., Volk, C. M., Homan, C. D., Fierli, F., Di Donfrancesco, G., Ulanovsky, A., Ravegnani, F., Sitnikov, N. M., Viciani, S., D'Amato, F., Shur, G. N., Belyaev, G. V., Law, K. S., and Cairo, F.: In situ measurements of tropical cloud properties in the West African Monsoon: upper tropospheric ice clouds, Mesoscale Convective System outflow, and subvisual cirrus, Atmos. Chem. Phys., 11, 5569–5590, doi:10.5194/acp-11-5569-2011, 2011.

Frey, W., Borrmann, S., Fierli, F., Weigel, R., Mitev, V., Matthey, R., Ravegnani, F., Sitnikov, N. M., Ulanovsky, A., and Cairo, F.: Tropical deep convective life cycle: Cb-anvil cloud microphysics from high-altitude aircraft observations, Atmos. Chem. Phys., 14, 13223–13240, doi:10.5194/acp-14-13223-2014, 2014.

Gayet, J.-F., Ovarlez, J., Shcherbakov, V., Ström, M., Schumann, U., Minikin, A., Auriol, F., Petzold, A., and Monier, M.: Cirrus cloud microphysical and optical properties at southern and northern midlatitudes during the INCA experiment, J. Geophys. Res., 109, D20206, doi:10.1029/2004JD004803, 2004.

Gensch, I., Bunz, H., Baumgardner, D., Christensen, L., Fahey, D., Hermann, R., Lawson, P., Popp, P., Smith, J., Webster, C., Weinstock, E., Wilson, J., Peter, T., and Krämer, M.: Supersaturations, microphysics and nitric acid partitioning in a cold cirrus observed during CR-AVE 2006: an observation-modeling intercomparison study, Environ. Res. Lett., 3, 035003, doi:10.1088/1748-9326/3/3/035003, 2008.

Gettelman, A., Liu, X., Ghan, S. J., Morrison, H., Park, S., Conley, A. J., Klein, S. A., Boyle, J., Mitchell, D. L., and Li, J.-L.F.: Global simulations of ice nucleation and ice supersaturation with an improved cloud scheme in the Community Atmosphere Model, J. Geophys. Res., 115, D18216, doi:10.1029/2009JD013797, 2010.

Heymsfield, A. and Iaquinta, J.: Cirrus crystal terminal velocities, J. Atmos. Sci., 57, 916–938, 2000.

Heymsfield, A. J., Bansemer, A., Field, P. R., Durden, S. L., Stith, J. L., Dye, J. E., Hall, W., and Grainger, C. A.: Observations and parameterizations of particle size distributions in deep tropical cirrus and stratiform precipitating clouds: results from in situ observations in TRMM field campaigns, J. Atmos. Sci., 59, 3457–3491, 2002a.

Heymsfield, A. J., Lewis, S., Bansemer, A., and Iaquinta, J., Miloshevich, L. M., Kajikawa, M., and Twohy, C., and Poellot, M. R.: A general approach for deriving the properties of cirrus and stratiform ice cloud particles, J. Atmos. Sci., 59, 3–29, 2002b.

Heymsfield, A., Schmitt, C., and Bansemer, A.: Ice cloud particle size distributions and pressure-dependent terminal velocities from in situ observations at temperatures from 0° to 286 °C, J. Atmos. Sci., 20, 4123–4154, doi:10.1175/JAS-D-12-0124.1, 2013.

Hoose, C. and Möhler, O.: Heterogeneous ice nucleation on atmospheric aerosols: a review of results from laboratory experiments, Atmos. Chem. Phys., 12, 9817–9854, doi:10.5194/acp-12-9817-2012, 2012.

Jensen, E., Diskin, G., Lawson, Lance, P., S., Bui, T., Hlavka, D., McGill, M., Pfister, L., Toon, O., and Gao, R.: Ice nucleation and dehydration in the Tropical Tropopause Layer, P. Natl. Acad. Sci. USA, 110, 2041–2046, doi:10.1073/pnas.1217104110, 2013a.

Jensen, E., Lawson, P., Bergman, J. W., Pfister, L., Bui, T. P., and Schmitt, C. G.: Physical processes controlling ice concentrations in synoptically forced, midlatitude cirrus, J. Geophys. Res., 118, 5348–5360, doi:10.1002/jgrd.50421, 2013b.

Jones, H. M., Haywood, J., Marenco, F., O'Sullivan, D., Meyer, J., Thorpe, R., Gallagher, M. W., Krämer, M., Bower, K. N., Rädel, G., Rap, A., Woolley, A., Forster, P., and Coe, H.: A methodology for in-situ and remote sensing of microphysical and radiative properties of contrails as they evolve into cirrus, Atmos. Chem. Phys., 12, 8157–8175, doi:10.5194/acp-12-8157-2012, 2012.

Kärcher, B. and Lohmann, U.: A parameterization of cirrus cloud formation: homogeneous freezing of supercooled aerosols, J. Geophys. Res., 107, XLXV–XLXVI, doi:10.1029/2002JD003220, 2002.

Kärcher, B. and Lohmann, U.: A parameterization of cirrus cloud formation: heterogeneous freezing, J. Geophys. Res., 108, AAC 2-1–AAC 2-15, doi:10.1029/2002JD003220, 2003.

Kärcher, B., Hendricks, J., and Lohmann, U.: Physically based parameterization of cirrus cloud formation for use in global atmospheric models, J. Geophys. Res., 111, D01205, doi:10.1029/2005JD006219, 2006.

Kienast-Sjögren, E., Miltenberger, A. K., Luo, B. P., and Peter, T.: Sensitivities of Lagrangian modelling of mid-latitude cirrus clouds to trajectory data quality, Atmos. Chem. Phys., 15, 7429–7447, doi:10.5194/acp-15-7429-2015, 2015.

Koop, T., Luo, B., Tsias, A., and Peter, T.: Water activity as the determinant for homogeneous ice nucleation in aqueous solutions, Nature, 406, 611–614, 2000.

Korolev, A., Emery, E., Strapp, J., Cober, S., Isaac, G., Wasey, M., and Marcotte, D.: Small ice particles in tropospheric clouds: fact or artifact? Airborne Icing Instrumentation Evaluation Experiment, B. Am. Meteorol. Soc., 92, 967–973, doi:10.1175/2010BAMS3141.1, 2011.

Korolev, A., Emery, E., Strapp, J., Cober, S., and Isaac, G.: Quantification of the effects of shattering on airborne ice particle measurements, J. Atmos. Ocean. Tech., 92, 2527–2553, doi:10.1175/JTECH-D-13-00115.1, 2013.

Krämer, M., Schiller, C., Afchine, A., Bauer, R., Gensch, I., Mangold, A., Schlicht, S., Spelten, N., Sitnikov, N., Borrmann, S., de Reus, M., and Spichtinger, P.: Ice supersaturations and cirrus cloud crystal numbers, Atmos. Chem. Phys., 9, 3505–3522, doi:10.5194/acp-9-3505-2009, 2009.

Krämer, M., Twohy, C., Hermann, M., Afchine, A., Dhaniyala, S., and Korolev, A.: Aerosol and cloud particle sampling, in: Airborne Measurements for Environmental Research: Methods and Instruments, edited by: Wendisch, M. and Brenguier, J.-L., Wiley-VCH Verlag GmbH &Co. KGaA, 303–341, doi:10.1002/9783527653218.ch6, 2013.

Lawson, R., O'Connor, D., Zmarzly, P., Weaver, K., Baker, B., Mo, Q., and Jonsson, H.: The 2D-S (Stereo) probe: design and preliminary tests of a new airborne, high-speed, high-resolution particle imaging probe, J. Atmos. Ocean. Tech., 23, 1462–1477, 2006.

Luebke, A. E., Avallone, L. M., Schiller, C., Meyer, J., Rolf, C., and Krämer, M.: Ice water content of Arctic, midlatitude, and tropical cirrus – Part 2: Extension of the database and new statistical analysis, Atmos. Chem. Phys., 13, 6447–6459, doi:10.5194/acp-13-6447-2013, 2013.

Luebke, A., Afchine, A., Costa, A., Meyer, J., Rolf, C., Spelten, N., Avallone, L., Baumgardner, D., and Krämer, M.: The origin of midlatitude ice clouds and the resulting influence on their microphysical properties, Atmos. Chem. Phys. Discuss., 15, 34243–34281.

May, R.: Open-path, near-infrared tunable diode laser spectrometer for atmospheric measurements of H_2O, J. Geophys. Res., 103, 19161–19172, doi:10.1029/98jd01678, 1998.

McFarquhar, G., Heymsfield, A., Spinhirne, J., and Hart, B.: Thin and subvisual tropopause tropical cirrus: observations and radiative impact, J. Atmos. Sci., 57, 1841–1853, 2000.

McFarquhar, G., Schmid, B., Korolev, A., Ogren, J., Russell, P., Tomlinson, J., Turner, D., and Wiscombe, W.: Airborne instrumentation needs for climate and atmospheric research, B. Am. Meteorol. Soc., 92, 1193–1196, doi:10.1175/2011BAMS3180.1, 2011.

Meyer, J.: Ice Crystal Measurements with the New Particle Spectrometer NIXE-CAPS, Schriften des Forschungszentrums Jülich, Reihe Energie und Umwelt/Energy and Environment, vol. 160, ISBN:9783893368402, Forschungszentrum Jülich, Jülich, 2012.

Meyer, J., Rolf, C., Schiller, C., Rohs, S., Spelten, N., Afchine, A., Zöger, M., Sitnikov, N., Thornberry, T. D., Rollins, A. W., Bozóki, Z., Tátrai, D., Ebert, V., Kühnreich, B., Mackrodt, P., Möhler, O., Saathoff, H., Rosenlof, K. H., and Krämer, M.: Two decades of water vapor measurements with the FISH fluorescence hygrometer: a review, Atmos. Chem. Phys., 15, 8521–8538, doi:10.5194/acp-15-8521-2015, 2015.

Mitchell, D. L., D'Entrmont, R. P., and Lawson, R. P.: Inferring cirrus size distributions through satellite remote sensing and microphysical databases, J. Atmos. Sci., 67, 1106–1125, doi:http://dx.doi.org/10.1175/2009JAS3150.110.1175/2009JAS3150.1, 2010.

Möhler, O., Field, P. R., Connolly, P., Benz, S., Saathoff, H., Schnaiter, M., Wagner, R., Cotton, R., Krämer, M., Mangold, A., and Heymsfield, A. J.: Efficiency of the deposition mode ice nucleation on mineral dust particles, Atmos. Chem. Phys., 6, 3007–3021, doi:10.5194/acp-6-3007-2006, 2006.

Muhlbauer, A., Ackerman, T., Comstock, J., Diskin, G., Evans, S., Lawson, R., and Marchand, R.: Impact of large-scale dynamics on the microphysical properties of midlatitude cirrus, Journal of Geophysical Research: Atmospheres, 119, 3976–3996, doi:10.1002/2013JD020035, 2014.

Murphy, D. and Koop, T.: Review of the vapour pressure of ice and supercooled water for atmospheric applications, Q. J. Roy. Meteor. Soc., 131, 1539–1565, 2005.

Peter, T., Marcolli, C., Spichtinger, P., Corti, T., Baker, M., and Koop, T.: When dry air is too humid, Science, 314, 1399–1401, 2006.

Rolf, C., Krämer, M., Schiller, C., Hildebrandt, M., and Riese, M.: Lidar observation and model simulation of a volcanic-ash-induced cirrus cloud during the Eyjafjallajökull eruption, Atmos. Chem. Phys., 12, 10281–10294, doi:10.5194/acp-12-10281-2012, 2012.

Rolf, C., Grooß, J.-U., Spichtinger, P., Costa, A., and Krämer, M.: Forecasting and understanding cirrus clouds with the large scale Lagrangian microphysical model CLaMS-Ice, Atmos. Chem. Phys. Discuss., in preparation, 2015.

Rollins, A. W., Thornberry, T. D., Gao, R. S., Smith, J. B., Sayres, D. S., Sargent, M. R., Schiller, C., Krämer, M., Spelten, N., Hurst, D. F., Jordan, A. F., Hall, E. G., Vömel, H., Diskin, G. S.,

Podolske, J. R., Christensen, L. E., Rosenlof, K. H., Jensen, E. J., and Fahey, D. W.: Evaluation of UT/LS hygrometer accuracy by intercomparison during the NASA MACPEX mission, J. Geophys. Res.-Atmos., 119, 1915–1935, doi:10.1002/2013JD020817, 2014.

Sassen, K. and Benson, S.: A midlatitude cirrus cloud climatology from the facility for atmospheric remote sensing. Part II: Microphysical properties derived from lidar depolarization, J. Atmos. Sci., 58, 2103–2112, doi:10.1175/1520-0469(2001)058<2103:AMCCCF>2.0.CO;2, 2001.

Sassen, K., Wang, Z., and Liu, D.: Global distribution of cirrus clouds from CloudSat/Cloud-Aerosol Lidar and Infrared Pathfinder Satellite Observations (CALIPSO) measurements, J. Geophys. Res., 113, D00A12, doi:10.1029/2008JD009972, 2008.

Schiller, C., Krämer, M., Afchine, A., Spelten, N., and Sitnikov, N.: Ice water content in Arctic, midlatitude and tropical cirrus, J. Geophys. Res., 113, D24208, doi:10.1029/2008JD010342, 2008.

Spichtinger, P. and Gierens, K. M.: Modelling of cirrus clouds – Part 1a: Model description and validation, Atmos. Chem. Phys., 9, 685–706, doi:10.5194/acp-9-685-2009, 2009.

Spichtinger, P. and Krämer, M.: Tropical tropopause ice clouds: a dynamic approach to the mystery of low crystal numbers, Atmos. Chem. Phys., 13, 9801–9818, doi:10.5194/acp-13-9801-2013, 2013.

Voigt, C. E. A.: ML-CIRRUS – a field experiment on natural and aviation induced cirrus with the new German research aircraft HALO, B. Am. Meteorol. Soc., in preparation, 2015.

Wendisch, M., Pöschl, U., Andreae, M. O., Machado, L. A., Albrecht, R., Schlager, H., Rosenfeld, D., Buchholz, B., Ebert, V., Fisch, G., Curtius, J., Frank, F., Kohl,., Rose, D., Longo, K., Afchine, A., Costa, A., Krämer, M., Jaervinen, E., Schnaiter, M., Ehrlich, A., Jäkel, E., Krisna, T. C., Kanter, S., Rosenow, D., Werner, F., Mertes, S., Kästner, U., Dorf, M., Klimach, T., Krüger, M., Nillius, B., Pöhlker, C., Schneider, J., Schulz, C., Borrmann, S., Mahnke, C., Molleker, S., Weigel, R., Ewald, F., Kölling, T., Mayer, B., Zinner, T., Fix, A., Fütterer, D., Jurkat, T., Kenntner, M., Sauer, D., Stock, P., Voigt, C., Weinzierl, B., Ziereis, H., Barbosa, H., Artaxo, P., de Souza, R. A. F., and Yamasoe, M. A.: The ACRIDICON-CHUVA observational study of tropical convective clouds and precipitation using the new German research aircraft HALO, B. Am. Meteorol. Soc., 2015.

Table 1. Overview of campaigns and instruments. IWC: ice water content, RH_{ice}: relative humidity over ice, N_{ice}: ice crystal number concentration.

Aircraft	Locations	IWC	RH_{ice}	N_{ice}
Geophysica	Seychelles[1], Europe[2], Brazil[3], Australia[4], Africa[5]	FISH[a]	FLASH[c]	FSSP-100[i]
Learjet	Europe[6]	FISH[a]	OJSTER[d], SEAL[e]	FSSP-300[j]
WB-57	USA[7], Costa Rica[8]	CLH[b]	HWV[f], JLH[g]	CAPS[k], 2-DS[l]
BAe-146	UK[9]	NIXE-CAPS[m]	–	NIXE-CAPS[m]
HALO	Europe[10], Brazil[11]	NIXE-CAPS[m]	SHARC[hrs]	NIXE-CAPS[m]

The campaigns under 1–6 are described by Schiller et al. (2008); Krämer et al. (2009) and Finger et al. (2015), 7–8 by Luebke et al. (2013); Jensen et al. (2013b), 9 Jones et al. (2012), 10 Voigt (2015), 11 Wendisch et al. (2015).

[1] APE-THESEO 1999.
[2] ENVISAT 2002, EUPLEX 2003, ENVISAT 2003.
[3] TROCCINOX 2005.
[4] SCOUT-O_3 2005.
[5] AMMA 2006.
[6] CIRRUS 2003, CIRRUS 2004, CIRRUS 2006, AIRTOSS-ICE 2013.
[7] MidCix 2004, MACPEX 2011.
[8] TC-4 2007.
[9] COALESC 2011.
[10] ML-CIRRUS 2014.
[11] ACRIDICON-CHUVA 2014.

[a] Lyman-α fluorescence hygrometer (Schiller et al., 2008; Krämer et al., 2009; Meyer et al., 2015).
[b] Tunable diode laser hygrometer (Luebke et al., 2013).
[c] Lyman-α fluorescence hygrometer (Krämer et al., 2009).
[d] Tunable diode laser hygrometer (Krämer et al., 2009).
[e] Tunable diode laser hygrometer (Buchholz et al., 2013).
[f] Lyman-α fluorescence hygrometer (Rollins et al., 2014).
[g] Tunable diode laser hygrometer (May, 1998).
[hrs] Tunable diode laser hygrometer (Meyer et al., 2015).
[i] Light scattering cloud probe (Krämer et al., 2009).
[j] Light scattering cloud probe (Krämer et al., 2009).
[k] Light scattering and optical imaging cloud probe (Baumgardner et al., 2001).
[l] optical imaging cloud probe (Lawson et al., 2006).
[m] Light scattering and optical imaging cloud probe (Meyer, 2012; Luebke et al., 2015).

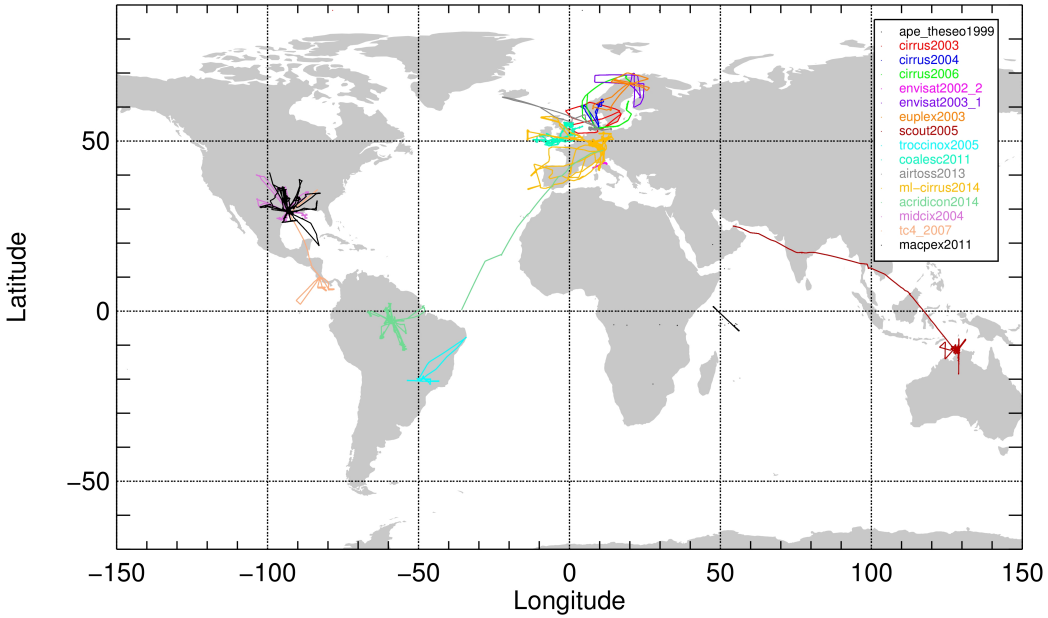

Figure 1. Aircraft flight paths during the campaigns listed above. Total number of flights: 104, total time of IWC measurements: 93.6 hrs.

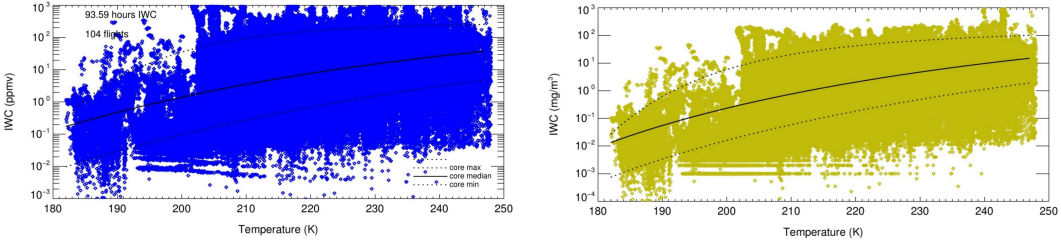

Figure 2. Observations of IWC vs. temperature during the flights shown in Fig. 1 (left: mixing ratio, right: concentration). Lines: median IWC (solid) and upper and lower bound of core IWC band (dotted) from observations of Schiller et al. (2008); Luebke et al. (2013). Total flight distance in clouds was about 67.390 km $\approx$ 336.960 data points (all data are sampled at 1 Hz).

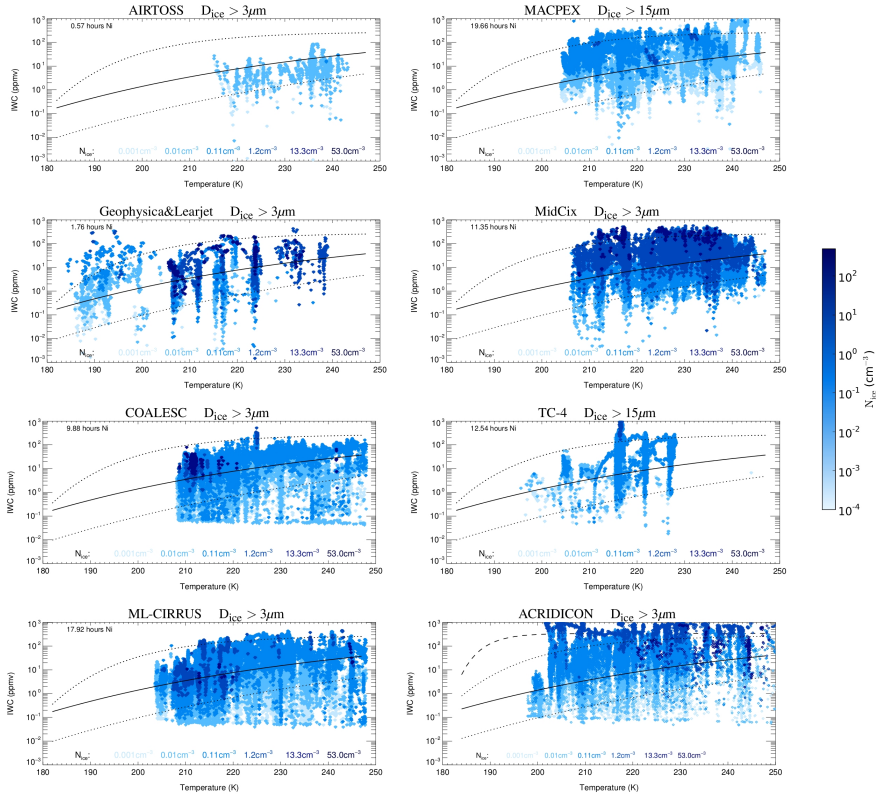

Figure 3. Observations of IWC vs. temperature, color coded by N_{ice} (= total number of ice crystals $> D_{\text{ice}}$). Left column: European field campaigns, right column: US/Brazil field campaigns. Total simultaneous IWC-N_{ice} measurements 85.7 hrs. Solid line: median IWC, dotted lines: upper and lower bound of the core IWC band (from observations of Schiller et al., 2008; Luebke et al., 2013). For instrumentation and campaigns see Table 1 and Fig. 1.

Single scenario

- Temperature range
  190 - 230 K
  in 10 K steps
- H_2O_{init}(T):
  90% RH_{ice}
- Vertical velocities:
  0.0001, 0.01, 0.1,
  0.5, 1.0, 3.0 m/s

➤ each scenario
contains
27 model runs

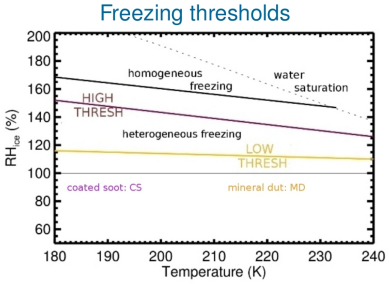

Scenarios

- HOM
- HET+HOM :
  - Ice nuclei (IN):
    0.001, 0.01, 0.1, 1.0 cm^{-3}
  - High/low freezing thresholds
- sedimentation parameter
  f = 0.9 / 0.5
- temperature fluctuations
  fluct / nofluct

➤ 18 nofluct , 18 fluct scenarios
→ Cirrus Guide:
972 model runs

Figure 4. Description of the MAID Cirrus Guide scenarios.

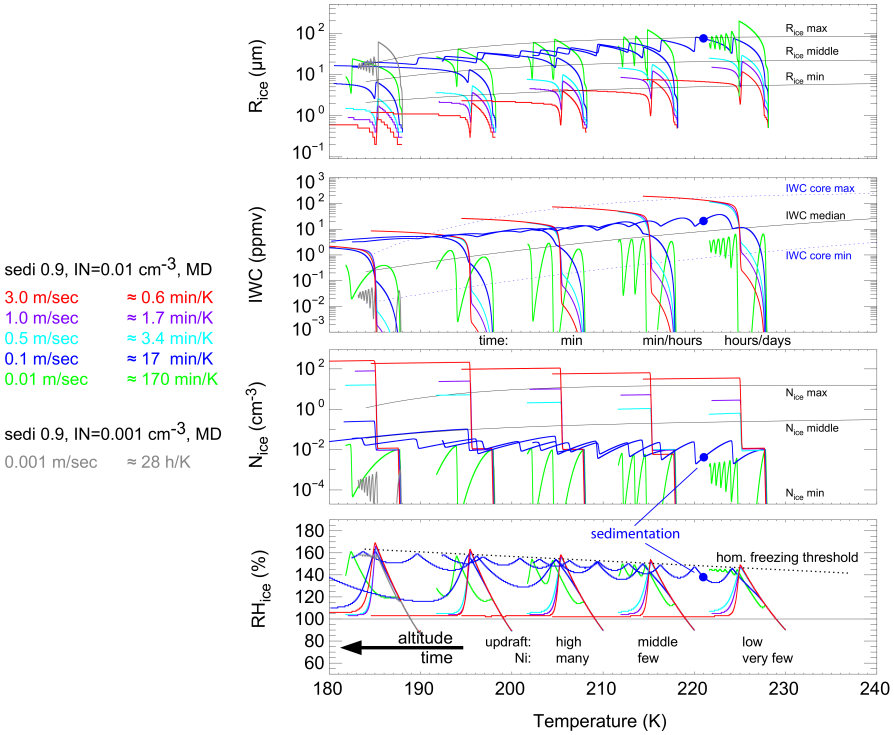

Figure 5. Cirrus scenario HET+HOM$|^{0.01-\mathrm{MD}}_{\mathrm{sedi}-0.9}$: simulated evolution of cirrus clouds at different temperatures and varying vertical velocities (see legend). The simulations propagate from right to left, the time of the simulations is indicated in the legend (in $\mathrm{min\,K^{-1}}$). Top panel: R_{ice} (lines: min, middle, max R_{ice} from Krämer et al. (2009)), 2nd panel: IWC (solid line: median IWC, dotted lines: upper and lower bound of the core IWC band from observations of Schiller et al. (2008); Luebke et al. (2013)), 3rd panel: N_{ice} (lines: min, middle, max N_{ice} from Krämer et al. (2009)), bottom panel: $\mathrm{RH_{ice}}$.

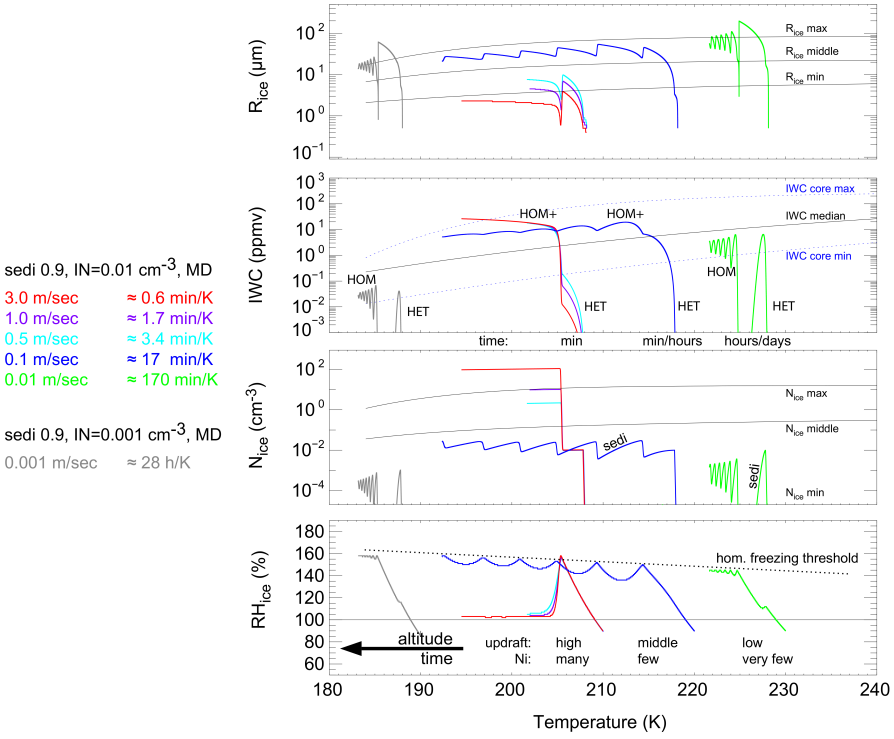

Figure 6. Same as Fig. 5, but only some selected trajectories are shown.

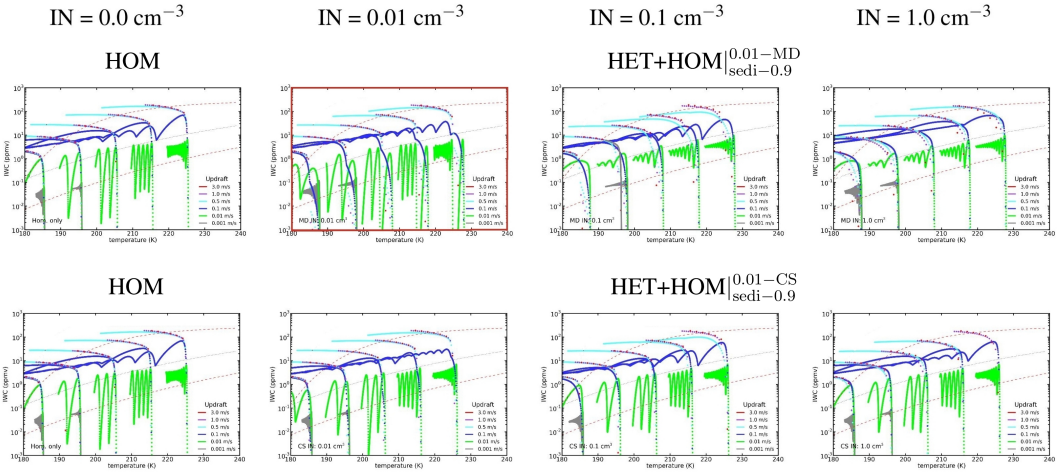

Figure 7. Cirrus scenarios in the IWC-Temperature parameter space for varying initial conditions, color coded by vertical velocities (color code see legend). Columns (from left to right): scenarios HOM (IN $= 0.0\,\mathrm{cm}^{-3}$) and HET + HOM (IN $= 0.01$, 0.1, $1.0\,\mathrm{cm}^{-3}$); top/bottom panels – freezing threshold MD/CS, sedi-f $= 0.9$ for all scenarios. Note that the IWC of the different vertical velocities is only weakly dependent on the different initial conditions. Solid line: median IWC, dotted lines: upper and lower bound of the core IWC band from observations of Schiller et al. (2008); Luebke et al. (2013).

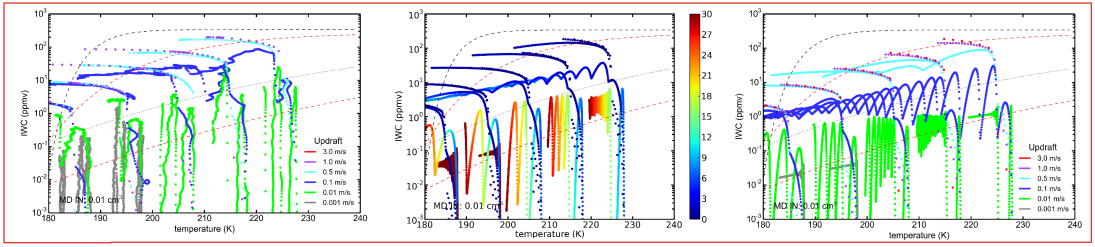

Figure 8. Cirrus scenario $\mathrm{HET} + \mathrm{HOM}|^{0.01-\mathrm{MD}}_{\mathrm{sedi}-0.9}$. Same as in Fig. 7 (red box) (and also Figs. 5 and 6), but: left: with superimposed temperature fluctuations, middle: color coded by time, right: with strong sedimentation (sedi $-$ 0.5).

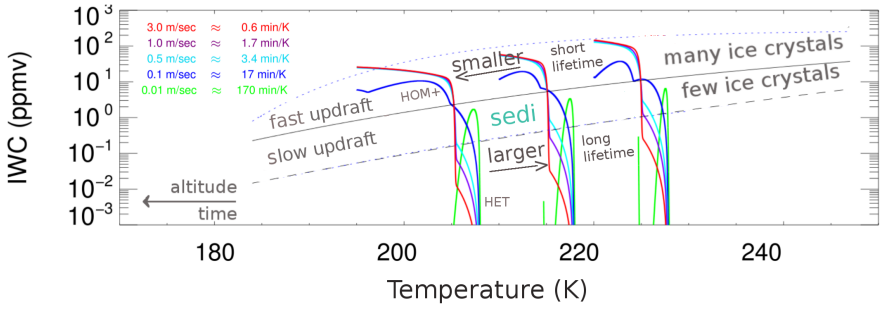

Figure 9. Sketch of the MAID in-situ Cirrus Guide: two classes of in-situ cirrus clouds are identified in the IWC-T parameter space. (1) IWCs below the median IWC line (Schiller et al., 2008; Luebke et al., 2013) mostly stem from **slow updraft cirrus**. They consist of few, but large ice crystals which are the larger the warmer the cirrus is. The first part of these cirrus is determined by HET freezing (indicated in the Figure). If the clouds life time is long enough, HOM freezing also starts. Due to the low updrafts, the number of ice crystals produced by HOM freezing does not greatly differ from the HET nucleated ice crystals. Thus, in slow updraft regions the difference in microphysics between HET and HOM formed cirrus is small. (2) High IWCs above the median IWC line are mostly produced by **fast updraft cirrus**. The time of the HET cirrus part at low IWC is short since the HOM freezing pushes the IWC quickly above the median line. With their large number of small, non-sedimenting ice crystals, these cirrus are microphysically very different from the slow updraft cirrus.

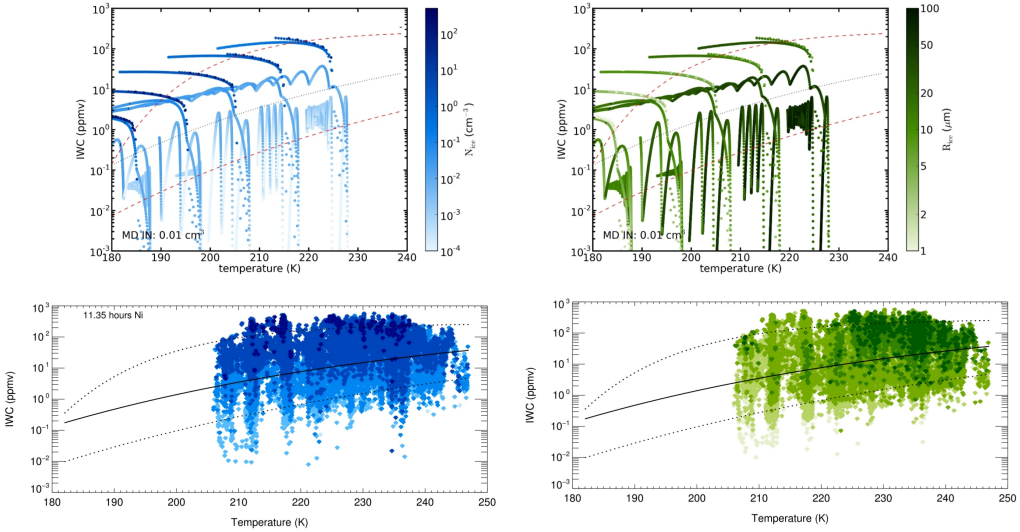

Figure 10. IWC colored by N_{ice} (left) and R_{ice} (right); top panels: MAID scenario $\text{HET} + \text{HOM}|^{0.01-\text{MD}}_{\text{sedi}-0.9}$, bottom panels: observations from MidCix.

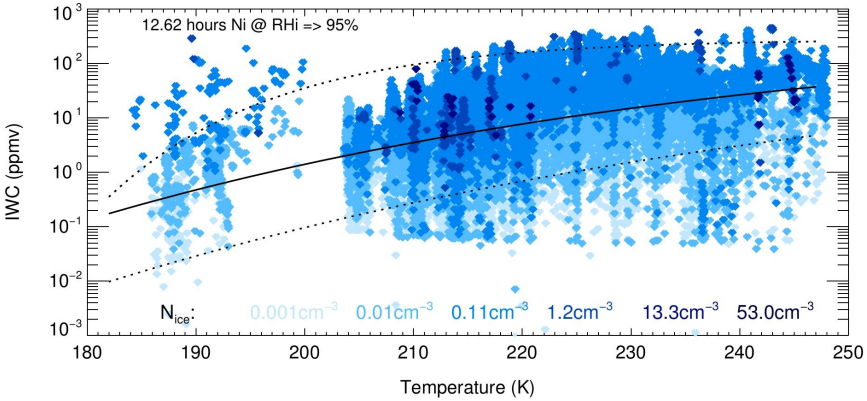

Figure 11. IWC colored by N_{ice} for (1) $\text{RH}_{\text{ice}} > 95\,\%$, which compares best to Cirrus Guide, and (2) those campaigns with PSDs for ice crystals with $D > 3\mu\text{m}$ and minimized ice crystal shattering effects (Geophysica – TTL flights, COALESC, AIRTOSS-ICE, ML-CIRRUS; ACRIDICON 2014 is not considered since it is nearly entirely driven by strong convection).

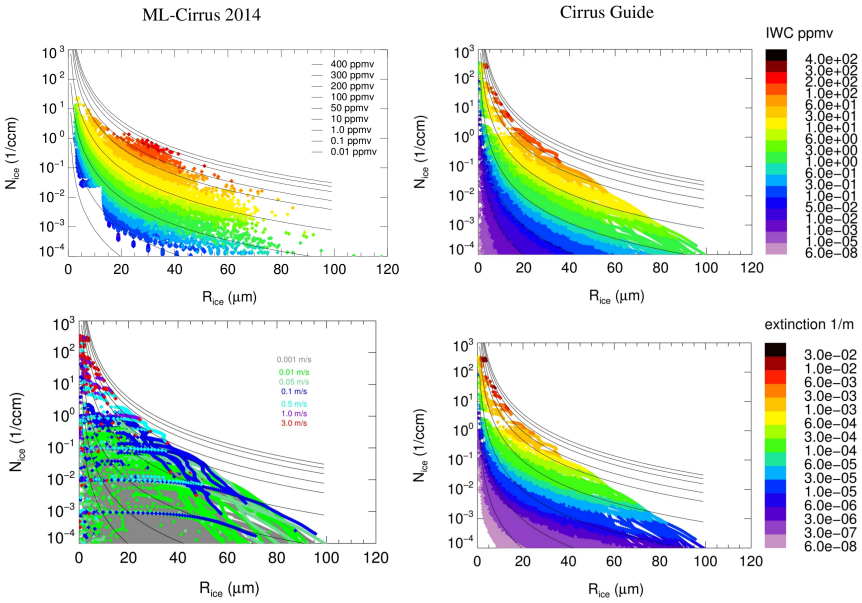

Figure 12. N_{ice} vs. R_{ice}. Upper left panel: observations of in-situ cirrus during ML-CIRRUS 2014 – color code IWC, black lines are IWC isolines. The other panels show the simulated Cirrus Guide: upper right – color code IWC, lower left – color code vertical velocity, lower right – color code extinction. The simulations contain all scenarios including temperature fluctuations ("fluct", see Sect. 3).

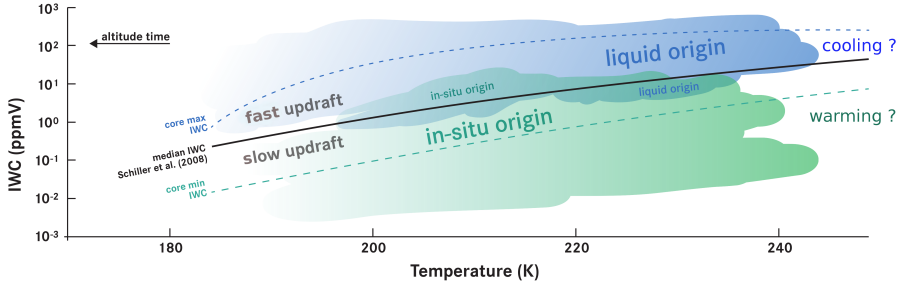

Figure 13. Sketch of in-situ and liquid origin cirrus (large letters: high frequency of occurrence, larger ice crystals, stronger sedimentation, longer lifetimes; small letters: low frequency of occurrence, smaller ice crystals, lesser sedimentation, shorter lifetimes). **In-situ origin cirrus** (greenish color): ice crystals form heterogeneously+homogeneously directly from the gas phase. In-situ cirrus are preferably thin with lower IWC. They divide in two classes (see also Fig. 9): (1) thin cirrus forming in slow updrafts consisting of few, large ice crystals with a large geographic coverage and a long lifetime, (2) thicker cirrus forming in fast updrafts consisting of many, small ice crystals with a smaller geographic coverage. **Liquid origin cirrus** (blueish color): ice crystals stem from frozen liquid drops which are uplifted from farther below in the atmosphere into the cirrus temperature range. Liquid origin cirrus are mostly thick with higher IWC and have larger ice crystals than the in-situ cirrus (for more detail see Luebke et al., 2015). Their geographic coverage/lifetime depend on the meteorological situation: larger/longer in warm conveyor belts, smaller/shorter in convective systems.